# Copyright Warning & Restrictions

The copyright law of the United States (Title 17, United States Code) governs the making of photocopies or other reproductions of copyrighted material.

Under certain conditions specified in the law, libraries and archives are authorized to furnish a photocopy or other reproduction. One of these specified conditions is that the photocopy or reproduction is not to be "used for any purpose other than private study, scholarship, or research." If a, user makes a request for, or later uses, a photocopy or reproduction for purposes in excess of "fair use" that user may be liable for copyright infringement,

This institution reserves the right to refuse to accept a copying order if, in its judgment, fulfillment of the order would involve violation of copyright law.

Please Note: The author retains the copyright while the New Jersey Institute of Technology reserves the right to distribute this thesis or dissertation

Printing note: If you do not wish to print this page, then select "Pages from: first page # to: last page #" on the print dialog screen

## ABSTRACT

## DRONE-ASSISTED EMERGENCY COMMUNICATIONS

**by**
**Di Wu**

Drone-mounted base stations (DBSs) have been proposed to extend coverage and improve communications between mobile users (MUs) and their corresponding macro base stations (MBSs). Different from the base stations on the ground, DBSs can flexibly fly over and close to MUs to establish a better vantage for communications. Thus, the pathloss between a DBS and an MU can be much smaller than that between the MU and MBS. In addition, by hovering in the air, the DBS can likely establish a Line-of-Sight link to the MBS. DBSs can be leveraged to recover communications in a large natural disaster struck area and to fully embody the advantage of drone-assisted communications. In order to retrieve signals from MUs in a large disaster struck area, DBSs need to overcome the large pathloss incurred by the long distance between DBSs and MBSs. This can be addressed by the following two strategies.

First, placing multiple drones in a disaster struck area can be used to mitigate the problem of large backhaul pathloss. In this method, data from MUs in the disaster struck area may be forwarded by more than one drone, i.e., DBSs can enable drone-to-drone communications. The throughput from the disaster struck area can potentially be enhanced by this multi-drone strategy. A cooperative DBS placement and channel allocation algorithm is proposed to maximize the aggregated data rate from MUs in a disaster struck area. It is demonstrated by simulations that the aggregated data rate can be improved by more than 10%, as compared to the scenario without drone-to-drone communications.

Second, free space optics (FSO) can be used as backhaul links to reduce the backhaul pathloss. FSO can provision a high-speed point-to-point transmission and is suitable for backhaul transmission. A heuristic algorithm is proposed to maximize the

number of MUs that can be served by the drones by optimizing user association, DBS placement and spectrum allocation iteratively. It is demonstrated by simulations that the proposed algorithm can cover over 15% more MUs at the expense of less than 5% of the aggregated throughput. Equipping DBSs and MBSs with FSO transceivers incurs extra payload for DBSs, hence shortening the hovering time of DBSs. To prolong the hovering time of a DBS, the FSO beam is deployed to facilitate simultaneous communications and charging. The viability of this concept has been studied by varying the distance between a DBS and an MBS, in which an optimal location of the DBS is found to maximize the data throughput, while the charging power directed to the DBS from the MBS diminishes with the increasing distance between them.

Future work is planned to incorporate artificial intelligence to enhance drone-assisted networking for various applications. For example, a drone equipped with a camera can be used to detect victims. By analyzing the captured pictures, the locations of the victims can be estimated by some machine learning based image processing technology.

# DRONE-ASSISTED EMERGENCY COMMUNICATIONS

by
Di Wu

A Dissertation
Submitted to the Faculty of
New Jersey Institute of Technology
in Partial Fulfillment of the Requirements for the Degree of
Doctor of Philosophy in Electrical Engineering

Helen and John C. Hartmann Department of
Electrical and Computer Engineering

December 2020

**APPROVAL PAGE**

**DRONE ASSISTED EMERGENCY COMMUNICATIONS**

**Di Wu**

---

Dr. Nirwan Ansari, Dissertation Advisor Date
Distinguished Professor, Helen and John C. Hartmann Department of Electrical and Computer Engineering, NJIT

---

Dr. Sui-Hoi Edwin Hou, Committee Member Date
Professor, Helen and John C. Hartmann Department of Electrical and Computer Engineering, NJIT

---

Dr. Abdallah Khreishah, Committee Member Date
Asspciate Professor, Helen and John C. Hartmann Department of Electrical and Computer Engineering, NJIT

---

Dr. Roberto Rojas-Cessa, Committee Member Date
Professor, Helen and John C. Hartmann Department of Electrical and Computer Engineering, NJIT

---

Dr. Guiling Wang, Committee Member Date
Professor, Ying Wu College of Computing, Department of Computer Science, NJIT

## BIOGRAPHICAL SKETCH

**Author:** Di Wu

**Degree:** Doctor of Philosophy

**Date:** December 2020

**Undergraduate and Graduate Education:**

- Doctor of Philosophy in Electrical Engineering,
  New Jersey Institute of Technology, Newark, NJ, 2020
- Master of Science in Electrical Engineering,
  Harbin Institute of Technology, Heilongjiang, China, 2015
- Bachelor of Science in Electrical Engineering,
  Harbin Institute of Technology, Heilongjiang, China, 2013

**Major:** Electrical Engineering

**Presentations and Publications:**

**D. Wu**, X. Sun and N. Ansari, "An FSO-based Drone Assisted Mobile Access Network for Emergency Communications," *IEEE Transactions on Network Science and Engineering*, vol. 7, no. 3, pp. 1597-1606, 1 July-Sept. 2020, doi: 10.1109/TNSE.2019.2942266.

**D. Wu** and N. Ansari, "A Cooperative Computing Strategy for Blockchain-secured Fog Computing," *IEEE Internet of Things Journal*, vol. 7, no. 7, pp. 6603-6609, July 2020, doi: 10.1109/JIOT.2020.2974231.

N. Ansari, **D. Wu**, and X. Sun, "FSO as Backhaul and Energizer for Drone-assisted Mobile Access Networks." *ICT Express (2020)*, vol. 6, no 2, pp. 139-144, doi: 10.1016/j.icte.2019.12.002

**D. Wu**, X. Sun and N. Ansari, "A Cooperative Drone Assisted Mobile Access Network for Disaster Emergency Communications," in *IEEE Global Communications Conference (GLOBECOM)*, Waikoloa, HI, 2019, pp. 1-6, doi: 10.1109/GLOBECOM38437.2019.9013813.

**D. Wu** and N. Ansari, "High Capacity Spectrum Allocation for Multiple D2D Users Reusing Downlink Spectrum in LTE," in *IEEE International Conference on Communications (ICC)*, Kansas City, MO, 2018, pp. 1-6, doi: 10.1109/ICC.2018.8422778.

**D. Wu** and N. Ansari, "A Trust Evaluation Enhanced Blockchain-Secured Industrial IoT System," *IEEE Internet of Things Journal*, doi: 10.1109/JIOT.2020.3030689, early access.

**D. Wu**, X. Sun and N. Ansari, "An FSO-based Drone Charging System for Emergency Communications," *IEEE Transactions on Vehicular Technology*, (submitted).

*To my dear wife, my parents and parents in law. Their encouragement, sacrifices, unwavering support and love have meant more to me than they can imagine.*

## ACKNOWLEDGMENT

My deepest gratitude is to my advisor, Dr. Nirwan Ansari. I have been amazingly fortunate to have him give me the freedom and encouragement to explore research ideas while providing excellent guidance. His persistent support and patience helped me overcome many difficult situations throughout my research. Without his continuous help, this dissertation would not have been possible.

To my committee members, Dr. Abdallah Khreishah, Dr. Roberto Rojas-Cessa, Dr. Edwin Hou, and Dr. Guiling Wang, I thank them for their time and advisement.

This dissertation is based upon work supported by the National Science Foundation under Grant No. CNS-1814748.

I want to thank my friends: Xiang Sun, Xilong Liu, Shuai Zhang, Weiqi Liu, Jingjing Yao, and many others, who have given me support and encouragement over the last six years.

I would like to extend my gratitude to other faculty and staff members of the Department of Electrical and Computer Engineering for their support throughout my doctoral studies.

## TABLE OF CONTENTS

## TABLE OF CONTENTS
## (Continued)

**Chapter** **Page**

## LIST OF TABLES

**Table** **Page**

## LIST OF FIGURES

# CHAPTER 1

# INTRODUCTION

Owing to the high availability and high data rate provided by mobile networks, the number of mobile subscribers is increasing over the years [54]. According to Ericsson Mobility Report, the total number of mobile subscriptions was around 7.9 billions in Q3 2018 and was forecast to reach 8.9 billions by the end of 2024. However, the mobile network infrastructure, such as base stations (BSs) and power transmission lines (which transport electricity from the power grid to BSs), could be damaged owing to natural disasters. Consequently, mobile users (MUs) in a disaster-struck area (i.e., the area covered by malfunctioned BSs) are unable to connect to the network and obtain any services. How to quickly recover communications in the disaster-struck area is a very critical issue which has drawn much attention [44]. Quickly recovering communications can help people in disaster-struck areas transmit the disaster information out of the area. Thus, rescue personnel can make accurate evaluation of disasters and design efficient rescue plans [58]. In rescuing people afflicted by disasters, valid wireless communications can help reduce the searching area and enhance survivability [39].

There are many strategies to recover communications in disaster-struck areas. One method is to equip ground vehicles with radio head to conduct the function of ground movable BSs. Ground movable BSs can be deployed near the disaster-struck area to provision MUs with temporary communications by forwarding data between MUs and nearby working macro BSs (MBSs), which are located in the disaster-struck area; also, ground movable BSs can move to different locations upon requests [42, 47]. The drawbacks of applying ground movable BSs include [37] 1) inefficient deployment: deploying a ground movable BS to a designated destination may not

always be feasible as the road to the designated destination may be damaged; 2) limited wireless backhaul capacity: the deployed ground movable BS is considered as a relay node between MUs and a specific working MBS. The ground movable BS can be deployed in the disaster-struck area close to MSs, but the distance between a ground movable BS and a working MBS could be very long [38]. Also, the link between a working MBS and a ground movable BS may likely be on Non-Line of Sight (NLoS) [30]. Consequently, the pathloss between the ground movable BS and the working MBS may be very high, and limiting the wireless backhaul (between a ground movable BS and a working MBS) capacity. Note that the limited backhaul capacity may stifle the ground movable BS from relaying traffic from MUs to working MBSs [6].

In order to overcome the inefficient deployment and limited wireless backhaul capacity problem in the ground movable BSs strategy, drone-mounted base stations (DBSs), which act as relay nodes between MUs and working MBSs [55], can be deployed over the disaster-struck area. Different from ground movable BSs, DBSs can move in the air, and so can be deployed over the designated destination efficiently and flexibly [22]. Also, a DBS can hover at a high altitude to facilitate Line of Sight (LoS) for the wireless backhaul link between the DBS and its working MBS. In this case, the pathloss between the DBS and its working MBS is reduced, thus potentially increasing the wireless backhaul capacity [3]. Note that the wireless backhaul capacity is still very limited owing to the long distance between a DBS and its working MBS [23]. Also, the DBS can ferry traffic back to the working MBS. That is, a drone collects data from MUs, flies back to the working MBS, and transmits the collected data to the working MBS [36]. This method can mitigate the limited wireless backhaul capacity constraint, but it incurs a long communications delay caused by the latency of the DBS flying back to the working MBS.

The drone assisted system can really achieve a very quick deployment and help recover the communications. However, many issues are still to be addressed in order to provide a durable stable service, to serve more users and to improve the servce quality. First, how does one provide service to more users? Since DBSs can provide a high probability of establishing LoS between DBSs and MUs, the access link pathloss can be minimized accordingly. The LoS probability is determined by the altitude of the DBS and the horizontal distance between the DBS and a corresponding MU [1]. In a DBS-assisted wireless communications network, a good location of DBS can help the DBS serve more MUs with LoS links. Different from placing ground base stations, the placement of DBS needs to consider the altitude of DBSs and the power consumption. By satisfying the QoS of different MUs, the 3-D DBS placement strategy incurs a high complexity and it is very hard to acquire the optimal solution [25]. Second, how does one increase the backhaul data rate? A DBS is usually sent to provide service in the area that has weak cellular signals or has no cellular service. A DBS is acting as a relay node by collecting the data from MUs and transmitting the collected data to its corresponding MBS, and requiring a large backhaul data rate accordingly. In order to increase the backhaul data rate, the DBS can use a larger bandwidth or try to reduce the pathloss between the DBS and MBS. Since the DBS is usually using the licensed wireless band in this scenario which is very precious and limited, allocating more bandwidth to a DBS is not usually economically inviable [29]. Thus, reducing the pathloss is the main method of increasing the backhaul data rate for DBSs. To satisfy the QoS of all served MUs, the LoS channel between the DBS and the MBS may not be guaranteed, e.g., the link between a DBS at a low altitude and a MBS in urban area has a high probability of being blocked by buildings. In this case, the placement of DBSs can influence the backhaul data rate. Apart from the placement of DBSs, new transmission technologies can also be used to increase the backhaul data rate. The beam forming technology [60] can provide

a directional RF beam with small scattering angle. Deploying a massive MIMO antenna at the DBS will increase the payload and the power consumption, which may significantly reduce the DBS hovering time. Optical wireless communications, which incurs a low pathloss and provisions a high point-to-point data rate, is used to provide backhaul communications in DBSs. Optical communications requires optical transceivers, which incur extra payloads for drones and may reduce the hovering time of drones. We can conclude that reducing the pathloss between DBSs and MBSs without incurring unnecessary extra payloads is a big challenge for drone assisted networks. Third, how does one extend the service time of a DBS? Based on the current battery technology, the hovering time of a commercial drone is usually around 30 minutes. Considering the extra power consumption of a DBS, e.g., the energy for forwarding RF signals and the energy for computing, the actual service time of a DBS is less than 30 minutes. Obviously, 30 minutes of service time may be suitable for some emergency communications, but are not enough for some missions that require longer service time. One current solution is leveraging some wireless charging technologies to extend the hovering time of a drone. Even the charging power is limited, especially in comparison with the power consumption of drones, using wireless charging remains an achieveable method to extend the hovering time of drones. Wireless charging may extend the hovering time of a drone for only a few minutes. In some scenarios, a few more minutes can be critical for a drone-assisted network. In current wireless charging strategy, how to achieve a high efficient charging rate to extend the hovering time is a critical issue.

The rest of this thesis is organized as follows. In Chapter 2, the architecture of a DBS assisted network is proposed. In the architecture, several working MBS are around the disaster struck area that can provide service to the DBSs. The number of DBSs in the disaster struck area is the same as the number of MBSs. Each DBS is serving a number of MUs on the ground. In Chapter 3, a multi-drone network

architecture in a disaster-struck area is proposed, in which multiple drones can communicate with each other directly. Thus, the drones burdened with heavy access link traffic can forward their traffic to other drones with light traffic. The optimization problem is formulated to maximize the throughput from the MUs to MBSs and the COoperative DBS plAcement and CHannel allocation (COACH) algorithm is proposed to solve the problem. The performance of COACH is demonstrated via simulations. In Chapter 4, using the free space optics (FSO) link to replace the RF link between MBSs and DBSs is investigated. By using the FSO in backhaul links, the data rate capacity between between an MBS and a DBS is much higher than using RF. The low pathloss of FSO link allows DBSs hovering far from MBSs to serve MUs. The problem of providing service to more MUs with FSO backhaul link is formulated. Also, a QoS awaRe dronEbase Station plaCement and mobile User association stratEgy (RESCUE) is proposed to solve the problem by adjusting the bandwidth allocation, DBS placement and user association iteratively. To extend the hovering time, the architecture of using FSO charging the DBS, based on the Free Space Optics as Backhaul and Energizer for Drone-Assisted Networking (SoarNet) architecture [7], is investigated. The performance of RESCUE and FSO charging are demonstrated via extensive simulations. A briefly introduction of future research endeavors is discussed in Chapter 5. The conclusion is presented in Chapter 6.

# CHAPTER 2

# DRONE-ASSISTED NETWORK ARCHITECTURE

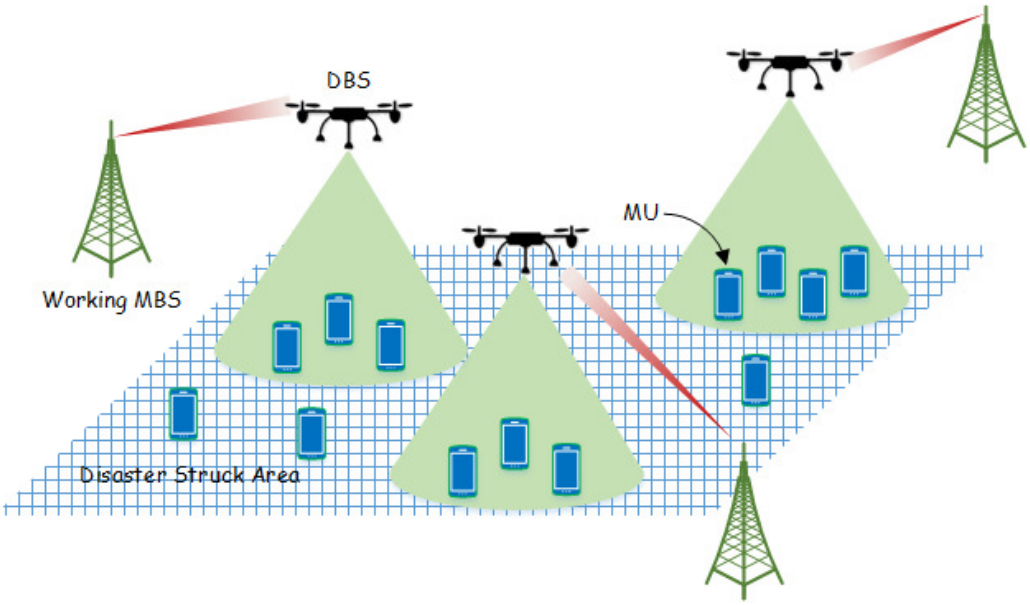


**Figure 2.1** Drone-assisted mobile access network.

To use drones in the disaster-struck areas, the architecture of multi-drone assisted network in a disaster-struck area is proposed and shown in Figure 2.1. Assuming that all MBSs in this disaster-struck area are out of service. Several DBSs are placed into this area to provide service to MUs. Each DBS is able to communicate with at least one MBS that is located outside this disaster-struck area. These MBSs outside the disaster-struck area are named as "working MBSs". However, considering the scale of the disaster-struck area and the coverage of DBSs, not all MUs in the disaster struck area are guaranteed to be served.

## 2.1 Isolated/Cooperative Drone-Assisted Networks

Based on different drone communications strategies, the drone-assisted network can be considered as cooperative and isolated.

In an isolated drone-assisted network, the main function of a DBS is to forward data from MUs to the working MBS. DBSs in one disaster-struck area cannot communicate with other DBSs directly [26]. Each DBS only communicates with it served MUs and forward the data to its associated working MBS. In this case, the management (including the placement and resource allocation) of each DBS is determined by its associated working MBS, and incurs no communications between DBSs. Even each DBS is prefered to be placed close to its associated working MBS while satisfying the QoS quirement of its served MUs, the coverage of different DBSs may overlap, especially with many DBSs serving in a small disaster struck area [45]. Thus, the isolated drone-assisted network usually covers a large disaster struck area.

In a cooperative drone-assisted network, DBSs may establish device-to-device (D2D) communications links with other DBSs. In this case, one DBS can not only forward data from the MUs in its own coverage to the working MBS, but can also forward the data from other DBSs. In a disaster struck area with varying MU density, the data rates from the served MUs vary as well [62]. Based on different DBS placement strategies (e.g., to cover more MUs in the disaster struck area), some DBSs may experience congestion in the backhaul (i.e., the total data rate from the access link is larger than the achieveable backhaul data rate). With the cooperative transmission strategy, the DBS with a congested backhaul may forward the data to those uncongested DBSs in order to achieve a higher throughput from MUs to MBSs in drone-assisted networks [46].

## 2.2 Backhaul Transmission in Drone-Assisted Networks

The backhaul transmission is a point-to-point transmission, and the radio frequency (RF) transmission is not the only choice for the backhaul link. Currently, the backhaul communication is mainly facilitated by RF and FSO.

RF backhaul is commonly deployed in drone-assisted systems. A DBS can use the same equipment to communicate with MBS and MUs. By using beam forming with antenna matrix in RF transmission, the MBS and the DBS can make a directional signal to significantly reduce the pathloss [57]. Since RF is a one-to-multiple transmission technology, the performance of RF is not as good as the technologies designed for point-to-point communications. Using RF as backhaul, the DBSs cannot be placed far from the working MBS [52].

FSO has recently been proposed to serve as the backhaul for a drone-assisted system. The FSO transmission is a point-to-point transmission technology designed for high speed transmission. To use FSO communications as backhaul links, an FSO transceiver is deployed in a DBS to transmit/receive optical signals from/to a working MBS [40]. The FSO backhaul system will incur some extra payload for the DBS for carrying the FSO transceiver, but the huge backhaul data rate capacity will potentially compensate for this extra payload. Different from RF signals, FSO signals are highly susceptible to the weather (e.g., the visibility range, the air humidity, etc.). In clear weather (e.g., the visibility range is larger than 1 km), the pathloss is very low and does not affect the transmission distance much. While in a foggy whether (e.g., the visibility range is smaller than 200 m), the pathloss is high influenced by the transmission distance [2]. The other characteristic of the FSO backhaul is its directivity, i.e., the LoS link between a DBS and an MBS. The optical beam is a highly directional beam, thus the FSO signal cannot be blocked by obstacles along its transmission path. Considering the high altitude of a DBS, the link between a DBS and its associated working MBS has a very high probability of being LoS [34]. By expounding on the above properties, the FSO backhaul is a very promissing wireless backhaul technology, especially for long distance transmission.

# CHAPTER 3

# COOPERATIVE DRONE-ASSISTED NETWORK

In the hovering mode drone-assisted network (i.e., a DBS will hover over a designated location, receive data from MUs via wireless access links, and forward data to a nearby working MBS via the wireless backhaul link), the wireless backhaul link between a DBS and a working MBS may become the bottleneck of uploading MUs' data to a working MBS, and it can significantly reduce the overall throughout. To solve the unbalanced backhaul throughput in a multi-drone assisted network, a mobile access network architecture empowered with multiple cooperative drones is proposed to deploy multiple DBSs in a disaster-struck area. A DBS may relay data not only from its MUs, but also from its neighboring DBSs via DBS-to-DBS (D2D) communications. As shown in Figure 3.1, each DBS communicates with its nearby working MBS to upload MUs' traffic. Assume that the wireless backhaul link between DBS 1 and working MBS 1 is the bottleneck, i.e., the capacity of the access links between DBS 1 and its MUs is larger than the capacity of the backhaul link between DBS 1 and its MBS. Then, DBS 1 can offload some traffic to DBS 2 via D2D communications. DBS 2 transmits the received traffic to its MBS via its backhaul link, which is not the bottleneck. Here, MUs are uploading data streams to working MBSs via deployed DBSs. The wireless backhaul link between a DBS and a working MBS may become the bottleneck of uploading MUs' data to a working MBS, thus significantly reducing the overall throughout.

## 3.1 System Model

In the drone-assisted mobile access network architecture with multiple cooperative drones, as shown in Figure 3.1, there are a number of DBSs available to be deployed over a disaster-struck area. Each DBS is to receive data from its associated MUs

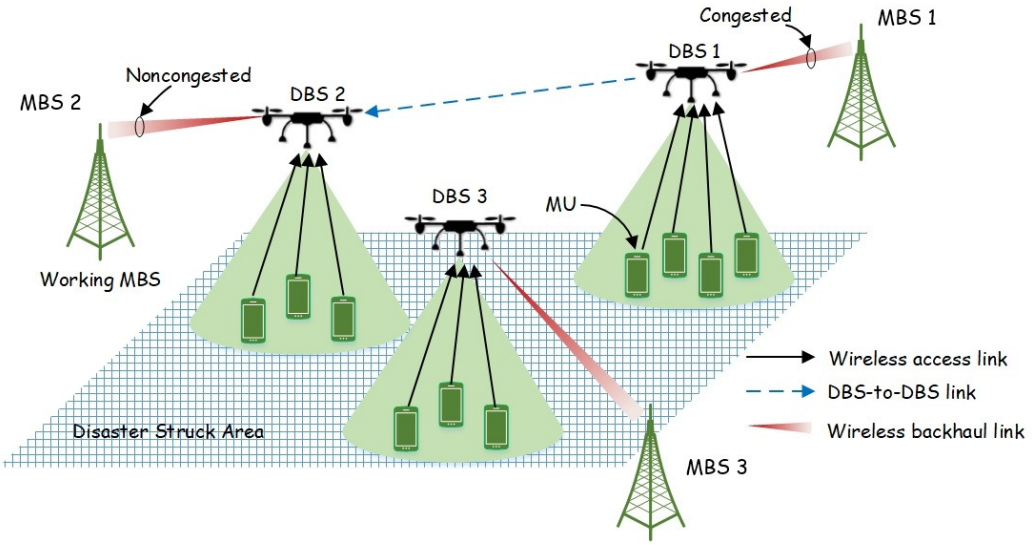


**Figure 3.1** Cooperative drones assisted mobile access network architecture.

via wireless access links, receive/transmit data from/to other DBSs via D2D links, and transmit the received data to its associated MBS via the wireless backhaul link. Denote $\boldsymbol{I}$ and $\boldsymbol{J}$ as the set of DBSs and MUs in the disaster-struck area, respectively, and $i$ and $j$ are used to index these DBSs and MUs, respectively.

Each DBS is connected to a dedicated MBS, and each DBS is operated in the in-band full-duplex mode, i.e., the backhaul link (from a DBS to its MBS) and the access links (from MUs to their DBSs) can transmit data simultaneously over the same frequency band [43]. Note that different DBSs are assigned with different spectrum bands but with the same amount of bandwidth to enable their own access and backhaul communications.

For DBS $i \in \boldsymbol{I}$, its allocated frequency band is equally divided into a number of channels. Denote $\boldsymbol{K}_i$ as the set of these channels allocated to DBS $i$ and $k$ is used to index these channel. $\lambda$ is the bandwidth of each channel. Denote $u_{jk}$ as the binary variable to indicate whether channel $k$ is allocated to MU $j$ in uploading its data (i.e., $u_{jk} = 1$) or not (i.e., $u_{jk} = 0$). Denote $v_{ik}$ as the binary variable to indicate whether channel $k$ is allocated to DBS $i$ in conducting backhaul communications or

not. Denote $w_{ii'k}$ as the binary variable to indicate whether channel $k$ is allocated to DBS $i$ and DBS $i'$ for D2D communications or not. If channel $k \notin \boldsymbol{K}_i$, then $\forall i \in \boldsymbol{I}, j \in \boldsymbol{J}$, $v_{ik} = u_{jk} = 0$.. Denote $\boldsymbol{K}$ as the set of all channels, i.e., $\boldsymbol{K} = \bigcup_{i \in \boldsymbol{I}} \boldsymbol{K}_i$.

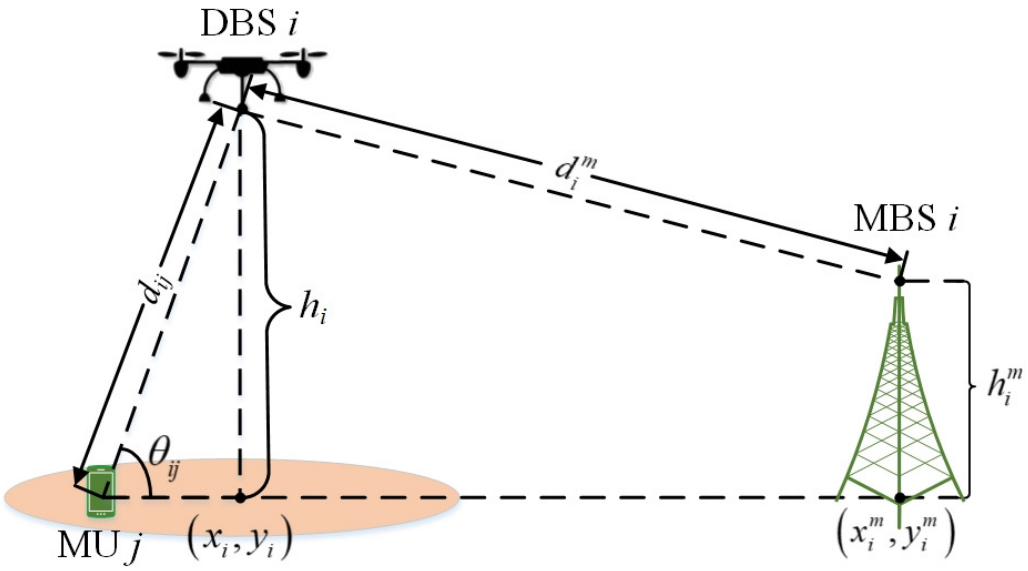


**Figure 3.2** Geometric relevance architecture.

### 3.1.1 D2D communications model

Links between DBSs are also considered as free space transmission, thus the pathloss between DBS $i$ and DBS $i'$ (where $i' \in \boldsymbol{I}$) is

$$\eta_{ii'}^d = 20 \log \left( \frac{4\pi f_{ii'} d_{ii'}^d}{c} \right), \tag{3.1}$$

where $f_{ii'}$ is the carrier frequency used between DBS $i$ and $i'$, and $d_{ii'}^d$ is the distance between DBS $i$ and DBS $i'$, i.e., $d_{ii'}^d = \sqrt{(x_i - x_{i'})^2 + (y_i - y_{i'})^2 + (h_i - h_{i'})^2}$.

D2D communications is conducted between DBS $i$ and DBS $i'$. As mentioned before, two DBSs are operated in two different spectrum bands to conduct their access and backhaul communications. Sender DBSs could reuse spectrum bands of receiver DBSs to achieve D2D communications. That is, any channel $k \in \boldsymbol{K}_{i'}$ can be used to conduct the communication from DBS $i$ to DBS $i'$. The data rate of transmitting

data from DBS $i$ to DBS $i'$ is acquired as:

$$r_{ii'}^{d} = \sum_{k \in \boldsymbol{K}_{i'}} (\lambda w_{ii'k} \log_2(1 + \tau_{ii'k}^{d})), \tag{3.2}$$

where $\tau_{ii'k}^{d}$ is the SINR between DBS $i$ and DBS $i'$ over channel $k$ ($k \in \boldsymbol{K}_{i'}$), i.e.,

$$\tau_{ii'k}^{d} = \frac{p_i g_{ii'}^{d}}{\lambda N_0 + \gamma p_{i'} v_{i'k}}, \tag{3.3}$$

where $g_{ii'}^{d}$ is the channel gain between DBS $i$ and DBS $i'$, i.e., $g_{ii'}^{d} = 10^{-\frac{\eta_{ii'}^{d}}{10}}$ (where $\eta_{ii'}^{d}$ is the pathloss between two DBSs, which is obtained from Equation (3.1)). Here, $\gamma p_{i'} v_{i'k}$ is the self-interference from DBS $i'$ in conducting backhaul communications if it uses the same channel $k$, where $p_{i'}$ is the transmission power of DBS $i'$ and $v_{i'k}$ is the indication of channel $k$ allocated to DBS $i'$ for its backhaul. Here, if channel $k$ is used for MU $j$ in uploading its data to DBS $i'$, channel $k$ cannot be used for the D2D communications, i.e.,

$$u_{jk} w_{ii'k} = 0, k \in \boldsymbol{K}_{i'}. \tag{3.4}$$

### 3.1.2 Access link communication model

The link between an MU and its associated DBS is normally modeled as a probabilistic LoS link. Denote the pathloss of having LoS and NLoS between DBS $i$ and MU $j$ (in dB) as $\eta_{ij}^{LoS}$ and $\eta_{ij}^{NLoS}$, respectively, where [3]

$$\eta_{ij}^{LoS} = 20 \log \left( \frac{4\pi f d_{ij}}{c} \right) + \xi_{ij}^{LoS}, \tag{3.5}$$

$$\eta_{ij}^{NLoS} = 20 \log \left( \frac{4\pi f d_{ij}}{c} \right) + \xi_{ij}^{NLoS}. \tag{3.6}$$

Here, $f$ is the carrier frequency, $c$ is the speed of light, $\xi_{ij}^{LoS}$ and $\xi_{ij}^{NLoS}$ are the additional losses for LoS and NLoS, respectively, and $d_{ij}$ is the distance between DBS $i$ and MU $j$, i.e.,

$$d_{ij} = \sqrt{(x_i - x_j)^2 + (y_i - y_j)^2 + h_i^2}, \tag{3.7}$$

where $< x_i, y_i, h_i >$ is the location of DBS $i$ and $< x_j, y_j >$ is the location of MU $j$. The probability of having LoS between DBS $i$ and MU $j$ can be estimated by [3]

$$\rho_{ij} = \frac{1}{1 + be^{-\beta(\theta_{ij} - b)}}, \tag{3.8}$$

where $b$ and $\beta$ are two environmental parameters in the disaster-struck area, and $\theta_{ij}$ is the elevation angle between DBS $i$ and MU $j$ (which is indicated in Figure 3.2), i.e., $\theta_{ij} = \arcsin\left(\frac{h_i}{d_{ij}}\right)$.

Based on Equation (3.5), (3.6), and (3.8), the pathloss between DBS $i$ and MU $j$, denoted as $\eta_{ij}^c$, can be modeled as [31]

$$\eta_{ij}^c = \rho_{ij}\eta_{ij}^{LoS} + (1 - \rho_{ij})\eta_{ij}^{NLoS}. \tag{3.9}$$

Note that DBS $i$ can communicate with MU $j$ if the average pathloss between MU $j$ and DBS $i$ is less than a predefined threshold $\eta^{th}$ (i.e., $\eta_{ij}^c < \eta^{th}$).

The data rate of MU $j$ in uploading its data to DBS $i$ is

$$r_{ij}^a = \sum_{k \in \boldsymbol{K}_i} (\lambda u_{jk} \log_2 (1 + \tau_{ijk})), \tag{3.10}$$

where $\tau_{ijk}$ is the SINR of DBS $i$ in receiving signal from MU $j$ over channel $k$, i.e.,

$$\tau_{ijk} = \frac{p_j g_{ij}}{\lambda N_0 + \gamma p_i}, \tag{3.11}$$

where $p_j$ is the transmission power of MU $j$ per channel, $N_0$ is the noise power, $\gamma$ is the self-interference parameter, $p_i$ is the transmission power of DBS $i$ per channel, and $g_{ij}$ is the channel gain between DBS $i$ and MU $j$, i.e., $g_{ij} = 10^{-\frac{\eta_{ij}^a}{10}}$, where $\eta_{ij}^a$ is the pathloss between DBS $i$ and MU $j$. For a clear exposition, the shadowing and fading effects are not considered in estimating the channel gain.

### 3.1.3 Backhaul communication model

Different from the channel between a DBS and an MU, the channel between a DBS and its associated working MBS is assumed to be free space [3]. Thus, the average pathloss between DBS $i$ and its MBS is

$$\eta_i^m = 20 \log \left( \frac{4\pi f d_i^m}{c} \right), \tag{3.12}$$

where $d_i^m$ is the distance between DBS $i$ and its MBS, i.e.,

$$d_i^m = \sqrt{(x_i - x_i^m)^2 + (y_i - y_i^m)^2 + (h_i - h_i^m)^2} \tag{3.13}$$

where $<x_i^m, y_i^m, h_i^m>$ is the 3-D position of DBS $i$'s associated working MBS.

The data rate from DBS $i$ to its MBS can be expressed as

$$r_i^b = \sum_{k \in \boldsymbol{K}_i} (\lambda v_{ik} \log_2(1 + \tau_i^b)), \tag{3.14}$$

where $\tau_i^b$ is the SNR for transmission from DBS $i$ to its associated MBS over any channel, i.e., $\tau_i^b = \frac{p_i g_i^b}{\lambda N_0}$. Here, $p_i$ is the transmission power of DBS $i$ per channel, $g_i^b$ is the channel gain between DBS $i$ and its associated MBS, i.e., $g_i^b = 10^{-\frac{\eta_i^b}{10}}$, and $\eta_i^b$ is the pathloss between DBS $i$ and its associated MBS. Note that DBS $i$'s associated MBS may receive interference from an MU (which is uploading data to DBS $i$ over channel $k$) or a DBS (which is transmitting data to DBS $i$ over channel $k$). Here, the interference is not considered, since the distance between DBS $i$ and its associated MBS is much shorter than the distance between MUs/other DBSs and DBS $i$'s associated MBS.

### 3.2 DBS Placement and Resource Allocation Strategy

Based on the system, the problem of maximizing the total throughput by DBS placement and spectrum allocation is formulated as follows.

$$\mathbf{P0:} \underset{u_{jk},v_{ik},w_{ii'k},x_i,y_i}{arg\max} \sum_{i\in\boldsymbol{I}}\sum_{j\in\boldsymbol{J}} r_{ij}^{a} \tag{3.15}$$

$$s.t.: C1: \sum_{j\in\boldsymbol{J}} r_{ij}^{a} + \sum_{i'\in\boldsymbol{I}\setminus i} r_{i'i}^{d} \le r_i^{b} + \sum_{i'\in\boldsymbol{I}\setminus i} r_{ii'}^{d}, \forall i \in \boldsymbol{I},$$

$$C2: u_{jk}w_{ii'k} = 0, \forall k \in \boldsymbol{K}_{i'}, \forall i, i' \in \boldsymbol{I}, \forall j \in \boldsymbol{J},$$

$$C3: \sum_{i\in\boldsymbol{I}} r_{ij}^{a} \ge r_j', \forall j \in \boldsymbol{J}, \exists u_{jk} \ne 0,$$

$$C4: u_{jk}, v_{ik}, w_{ii'k} \in \{0,1\}, \forall k \in \boldsymbol{K}_{i'}, \forall i, i' \in \boldsymbol{I}, \forall j \in \boldsymbol{J},$$

where the objective is to maximize the throughput of the network, C1 imposes the sum of the incoming data rate to be less than the sum of the outgoing data rate for each DBS, i.e., the backhaul link is not the bottleneck link. C2 imposes that Equation (3.4) is satisfied. C3 imposes that the provisioned data rate of MU $j$ to be larger than its data rate requirement, which is denoted as $r_j'$. C4 imposes that $u_{jk}$, $v_{ik}$, and $w_{ii'k}$ to be binary variables.

A heuristic algorithm, COoperative DBS plAcement and CHannel allocation (COACH), is designed to efficiently solve this optimization problem **P0**. The basic idea of COACH is to decompose **P0** into two sub-problems, i.e., DBS placement and channel allocation.

#### 3.2.1 DBS placement

The disaster-struck area is divided into a number of locations with the same size, denoted by set $\boldsymbol{N}$. If DBS $i$ is placed over location $n$ (where $n \in \boldsymbol{N}$), then the 2-D location of DBS $i$ (i.e., $< x_i, y_i >$) is the center of location $n$. The DBS placement is

**Algorithm 1** COACH

**for** all DBSs $i \in \boldsymbol{I}$ **do**

  **for** all locations $n \in \boldsymbol{N}$ **do**

    Obtain $\boldsymbol{J}_i^n$.

    Calculate $\bar{r}_i^a$ and $\bar{r}_i^b$ based on Eq. (3.17) and Eq. (3.18).

    Calculate $\bar{r}_i^n$ based Eq. (3.19)

  **end for**

  Select the best location $n^*$ for DBS $i$ based on Eq. (3.20).

  $\forall j \in \boldsymbol{J}_i^n$, calculate $z_{ij}$ based on Eq. (3.21).

  Allocate channels to MUs iteratively based on $g_{ij}$. Channel allocation terminates once $\sum_{j \in \boldsymbol{J}_i^n} z_{ij} \geq |\boldsymbol{K}_i|$ or all MUs are assigned channels.

  Remove the MUs (which are assigned channels) from $\boldsymbol{J}_i^n$.

  Calculate $r_i^a$ and $c_i^b$ based on Eq. (3.22) and Eq. (3.23).

**end for**

Divide DBSs into two sets, i.e., $\boldsymbol{I}^s$ and $\boldsymbol{I}^r$, where $\boldsymbol{I}^s = \left\{ i \in \boldsymbol{I} \,\middle|\, r_i^a > c_i^b \right\}$ and $\boldsymbol{I}^r = \left\{ i \in \boldsymbol{I} \,\middle|\, r_i^a < c_i^b \right\}$).

Derive the number of available channels for each DBS in $\boldsymbol{I}^r$ based on Eq. (3.24).

Calculate the data rate of all the possible D2D pairs based on Eq. (3.25).

Calculate the number of channels that could be allocated for all the possible D2D pairs based on Eq. (3.26).

**while** $\boldsymbol{I}^r \neq \emptyset$ and $\boldsymbol{I}^s \neq \emptyset$ **do**

  Select the D2D pair that incurs the maximum data rate and allocate the number of channels.

  Adjust the MU association of the source DBS for the selected D2D pair such that Constraint C1 is met.

  Remove the source and destination DBSs of the selected D2D pair from $\boldsymbol{I}^s$ and $\boldsymbol{I}^r$, respectively.

**end while**

to find the location that yields the maximum estimated data rate for MUs to upload their data streams.

Denote $\boldsymbol{J}_i^n$ as the set of MUs satisfying the channel gain threshold when DBS $i$ is at location $n$, (i.e., $g_{ij}^n > g_i^{th}$). The channel gain threshold defines the minimum channel gain between a DBS and an MU to enable communications. Assume that all MUs in $\boldsymbol{J}_i^n$ are associated to DBS $i$. The average channel gain between the MUs in $\boldsymbol{J}_i^n$ and DBS $i$ is defined as

$$\bar{g}_i^n = \sum_{j \in \boldsymbol{J}_i^n,} g_{ij}^n / |\boldsymbol{J}_i^n|. \tag{3.16}$$

Thus, the estimated access link data rate is defined as

$$\bar{r}_i^a = |\boldsymbol{K}_i| \lambda \log_2 \left(1 + \frac{p_j \bar{g}_i^n}{|\boldsymbol{K}_i| \lambda N_0}\right). \tag{3.17}$$

The data rate of the backhaul link between DBS $i$ and its MBS is defined as

$$\bar{r}_i^b = |\boldsymbol{K}_i| \, \lambda \log_2 \left(1 + \frac{p_i g_i^m}{|\boldsymbol{K}_i| \lambda N_0}\right), \tag{3.18}$$

where $g_i^m$ is the channel gain between DBS $i$ and its associated MBS. The estimated data rate of the MUs (in $\boldsymbol{J}_i^n$) in uploading their data to the MBS via DBS $i$, which is deployed over location $n$ ($\bar{r}_i^n$), is

$$\bar{r}_i^n = \min\left\{\bar{r}_i^a, \bar{r}_i^b\right\}. \tag{3.19}$$

DBS $i$ is placed over each location iteratively to find the location that incurs the maximum value of $\bar{r}_i^n$, i.e.,

$$n^* = \arg\max\left\{\bar{r}_i^n \,|n \in \boldsymbol{N}\right\}. \tag{3.20}$$

DBS $i$ will be placed over location $n^*$.

### 3.2.2 Resource allocation

**Access link channel allocation:** After placing DBS $i$, the associated MUs will be allocated channels. Note that MUs that cannot be served will be removed from $\boldsymbol{J}_i^n$. An MU unable to be served means that the wireless channels allocated to the MU are not enough to satisfy the data rate requirement of the MU.

The minimum number of channels for MU $j$ for uploading data to DBS $i$ (denoted as $z_{ij}$) in order to satisfy the data rate requirement of MU $j$ (i.e., C3) is

$$z_{ij} = \left\lceil \frac{r'_j}{\lambda \log_2 (1 + \tau_{ijk})} \right\rceil. \tag{3.21}$$

The available channels may not be enough to satisfy all the MUs' requirements. The MU, which incurs the highest channel gain to DBS $i$, will be assigned the channel first. The access link channel allocation will be terminated until all the MUs in $\boldsymbol{J}_i^n$ meet their requirements or there is no available channel.

The set of $\boldsymbol{J}_i^n$ is then updated by removing the MUs that are not assigned with channels in Step (b).

The data rate of DBS $i$ in receiving data from MUs ($r_i^a$) is

$$r_i^a = \sum_{j \in \boldsymbol{J}_i^n} r_{ij}^a, \tag{3.22}$$

where $r_{ij}^a$ is the data rate of MU $j$ in uploading data to DBS $i$. The capacity of the backhaul link between DBS $i$ and its MBS is

$$c_i^b = |\boldsymbol{K}_i| \lambda \log_2(1 + \tau_{ik}^m). \tag{3.23}$$

DBS $i$ may act differently in response to the following three scenarios: If $r_i^a < c_i^b$: DBS $i$ is not using all backhaul channels. Thus, DBS $i$ may help other DBSs offload their traffic by using D2D communications (i.e., DBS $i$ may be the receiver for D2D communications). When $r_i^a = c_i^b$: DBS $i$'s access link data rate just matches its

backhaul link capacity. That is, DBS $i$ does not have to offload its traffic to other DBSs; also, it cannot accept traffic offloaded from other DBSs. Otherwise, $r_i^a > c_i^b$: the backhaul link of DBS $i$ is the bottleneck, and so it has to offload traffic to other DBSs via D2D communications. That is, DBS $i$ could be the transmitter for D2D communications.

**DBS to DBS communications channel allocation:** After placing all DBSs and allocating access channels, the channels for D2D communications will be allocated. The placed DBSs can be divided into three sets, i.e., the set of DBSs with bottleneck backhaul links, i.e., $\boldsymbol{I}^s = \left\{i \in \boldsymbol{I} \,\middle|\, r_i^a > c_i^b\right\}$, the set of DBSs with their uncongested backhaul links, i.e. $\boldsymbol{I}^r = \left\{i \in \boldsymbol{I} \,\middle|\, r_i^a < c_i^b\right\}$, and the set of DBSs with their access link data rates just matched with their respective backhaul link capacities, i.e., $\boldsymbol{I}^o = \left\{i \in \boldsymbol{I} \,\middle|\, r_i^a = c_i^b\right\}$. D2D channel allocation is to select a DBS in $\boldsymbol{I}^s$ as the source node and a DBS in $\boldsymbol{I}^r$ as the destination node, and to allocate channels to offload traffic from the source node to the destination node.

A D2D communications pair (from DBS $i$ to DBS $i'$) uses the unused channels of DBS $i'$, i.e., if there are some unused channels in the destination node's access links, these channels can be used for D2D communications. The number of unused channels (in the access links) for each DBS in $\boldsymbol{I}^r$ is derived as

$$z'_{i'} = |\boldsymbol{K}_{i'}| - \sum_{j \in \boldsymbol{J}_{i'}^n} z_{i'j}. \tag{3.24}$$

Let $|\boldsymbol{I}^s|$ and $|\boldsymbol{I}^r|$ be the number of DBSs in $\boldsymbol{I}^s$ and $\boldsymbol{I}^r$, respectively. Thus, there are $|\boldsymbol{I}^s| \times |\boldsymbol{I}^r|$ number of possible pairs of D2D communications. For each possible D2D communications (from DBS $i$ to DBS $i'$), the average SINR is derived as $\tau_{ii'}^d = \sum_{k \in \boldsymbol{K}_{i'}} \frac{\tau_{ii'k}^d}{|\boldsymbol{K}_{i'}|}$, where $\tau_{ii'k}^d$ is calculated based on Equation (3.3). The data rate of D2D pair (DBS $i$ and $i'$) is

$$r_{ii'}^d = \lambda z_{ii'}^d \log_2(1 + \tau_{ii'}^d), \tag{3.25}$$

where $z^d_{ii'}$ is the number of channels used for D2D communications from DBS $i$ to $i'$, which depends on the number of unused channels in DBS $i'$'s access link (i.e., $z'_{i'}$ in Equation (3.24)) as well as the amount of traffic to be offloaded from DBS $i$ (i.e., $r^a_i - c^b_i$). The number of channels used for D2D communication from DBS $i$ to $i'$ ($z^d_{ii'}$) can be calculated as

$$z^d_{ii'} = \min\left\{z'_{i'}, \left\lceil \frac{r^a_i - c^b_i}{\lambda \log_2(1+\tau^d_{ii'})} \right\rceil \right\}, \tag{3.26}$$

where $\left\lceil \frac{r^a_i - c^b_i}{\lambda \log_2(1+\tau^d_{ii'})} \right\rceil$ is the number of required channels to offload $r^a_i - c^b_i$ amount of traffic from DBS $i$.

Then, we get the data rates of all possible D2D pairs by Equation (3.25). We pick the D2D pair with the maximum data rate, and allocate a number of channels (based on Equation (3.26)), and then remove the source DBS and the destination DBS in the D2D pair from $\boldsymbol{I}^s$ and $\boldsymbol{I}^r$, respectively. Note that, even D2D communications is enabled to offload the traffic from source DBS $i$ to destination DBS $i'$, source DBS $i$ still may not satisfy Constraint C1. If so, the MUs (which are associated with source DBS $i$) are iterarively dissociated from DBS $i$ to reduce access link traffic (i.e., the value of $r^a_i$) until $r^a_i \leq c^b_i + r^d_{ii'}$. The MU with a lower value of $r^a_{ij}$ will be disassociated from source DBS $i$ first.

### 3.2.3 Simulation results

Assume that six DBSs will be deployed over a disaster-struck area. The altitudes of DBSs are the same. There are 25 channels available for each DBS and the bandwidth of each channel is 180 kHz. The data rate requirements of MUs are generated based on a normal distribution, i.e., $N(2,1)$ $Mbps$. Other simulation parameters are listed in Table.3.1.

The results of COACH are compared to two other reference algorithms, i.e., access link aware (ALA) and backhaul link aware (BLA) DBS placement and channel

allocation. ALA is to maximize the access link data rate of a DBS without considering the backhaul link capacity. BLA is to maximize the overall throughput by jointly considering the access link data rate and the backhaul link capacity. Both algorithms do not apply D2D communications to offload traffic.

**Table 3.1** Simulation Parameters I

| | |
|---|---|
| Disaster area | 2 km × 2 km |
| Location area | 100 m × 100 m |
| Carrier frequency ($f$) | 2 GHz |
| Environment index ($b$) | 9.61 |
| Environment index ($\beta$) | 0.16 |
| $\xi^{LoS}$ | 1 dB [3] |
| $\xi^{NLoS}$ | 20 dB [3] |
| $\gamma$ | 130 dB [17] |
| $N_0$ | -104 dBm/Hz |
| $h_i^m$ | 30 m |
| $h_i$ | 50 m |

Figure 3.3 shows that the total data rate (of uploading data from MUs to MBSs) by varying the number of MUs. Note that the number of MUs in each location is selected based on a normal distribution, i.e., $N(\psi, 5)$, where $\psi$ is the average number of MUs in each location. $\psi$ is varied to adjust the number of MUs. COACH always yields the highest total data rate in the figure. However, as the number of MUs increases, the gap of the total data rate between COACH and BLA reduces because as the number of MUs is small, the backhaul link utilization incurred by BLA/ALA is not balanced among DBSs (e.g., some DBSs have 100% backhaul link utilization while some have the backhaul link utilization less than 80%); yet, COACH balances the backhaul link utilization by offloading the traffic from a DBS with congested backhaul

link to a DBS with uncongested backhaul link, and increases the total data rate. ALA is not affected much by the user density because ALA only maximizes the access link data rate without considering the backhaul link. In this case, the backhaul links have high probability of becoming bottleneck. However, as the number of MUs increases, the backhaul link utilization incurred by both ALA and BLA will be more balanced, as demonstrated in Figure. 3.4. That is, the link utilization of the backhaul, originally with less than 100%, is approaching 100%, thus reducing the average backhaul link utilization gap among COACH, ALA and BLA.

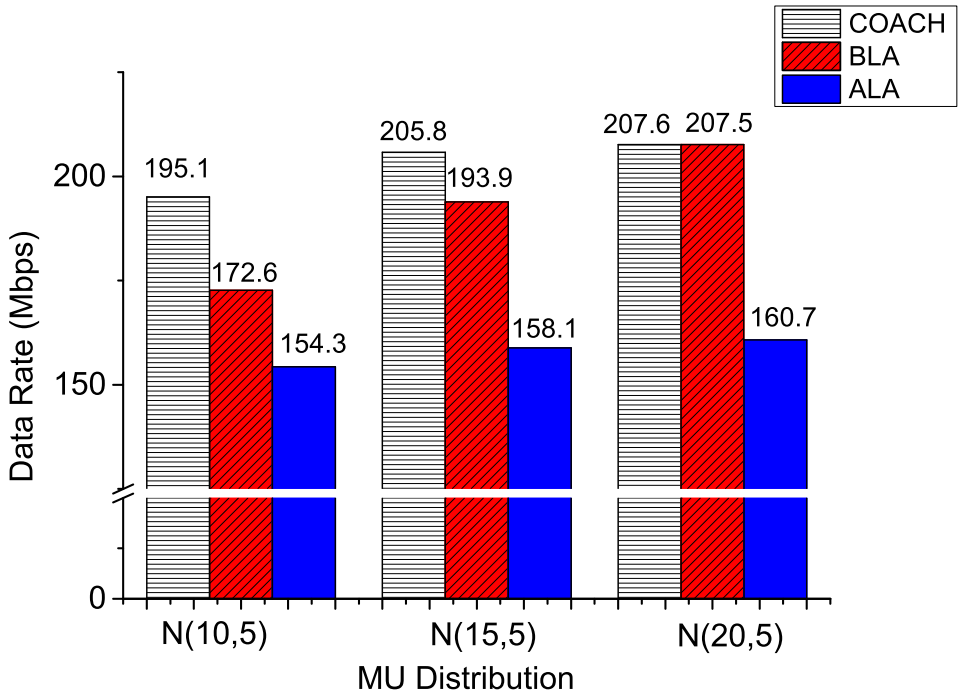


**Figure 3.3** Total data rate over different MU distributions.

The performance of different algorithms by varying the altitude of DBSs is shown in Figure 3.5. Note that the altitude of all MBSs is 30 $m$, and decreasing the altitude of a DBS from 50 $m$ to 30 $m$ essentially reduces the distance between the DBS and its associated MBS. Hence, the backhaul link between a DBS and its MBS has a better channel gain and provisions a larger backhaul link capacity.

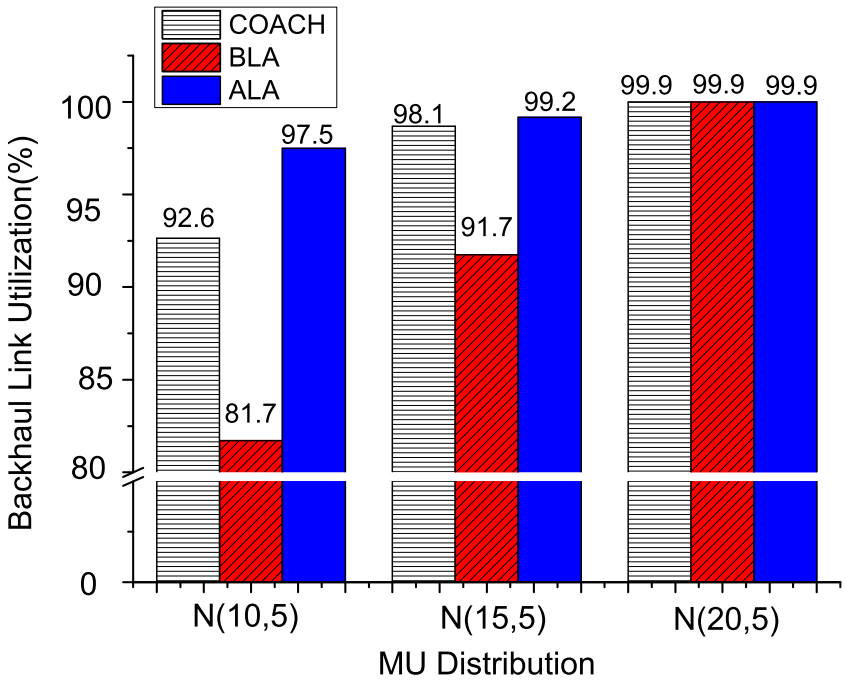


**Figure 3.4** Backhaul link utilization over different MU distributions.

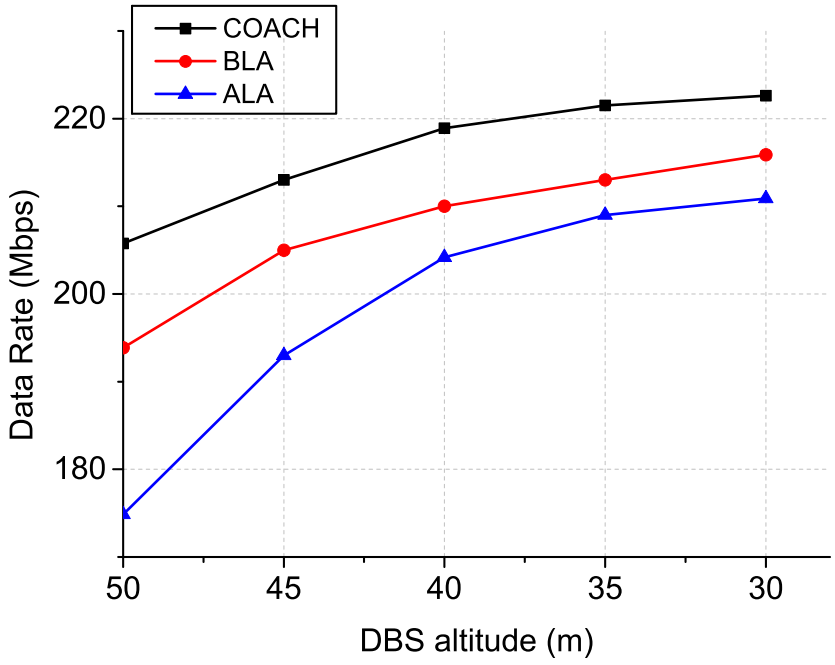


**Figure 3.5** Total data rate over different DBS altitudes.

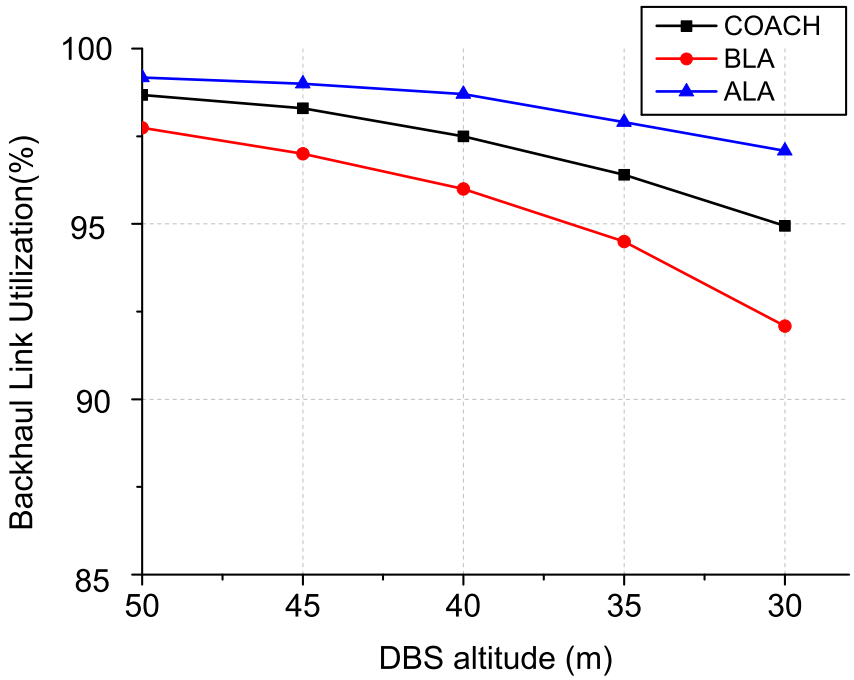


**Figure 3.6** Backhaul link utilization over different DBS altitudes.

In Figure 3.5, COACH incurs the highest data rate because it offloads traffic from congested backhaul links to uncongested backhaul links via D2D communications. Increasing the backhaul link capacity enables COACH to offload more traffic, and further increasing the overall throughput. BLA and ALA, on the other hand, do not offload traffic among backhaul links, and so incur lower data rates. Figure 3.6 shows how the altitude of the DBS affects the average backhaul link utilization. The average backhaul link utilization incurred by the three algorithms reduces as the altitude of the DBS decreases because decreasing the altitude of a DBS increases the capacity of the backhaul link, thus reducing the backhaul link utilization accordingly.

# CHAPTER 4

# FSO-BASED DRONE-ASSISTED NETWORK

In order to quickly recover communications in disaster-struck areas and achieve low communications delay between MUs and working MBSs, the FSO-based drone-assisted mobile access network architecture is proposed. As shown in Figure 4.1, a number of DBSs can be quickly deployed over the disaster-struck area. Note that the limited flying time of a battery-powered drone could be the major roadblock of deploying DBSs in the disaster-struck area. However, the flying time can be extended by applying gasoline-powered drones (which can last nearly one hour and get a fast refuel) or applying more than one drones to serve a group of MUs, e.g., two drones serving the same MUs iteratively. MUs in the disaster-struck area can associate to a specific DBS, which relays traffic between the nearby working MBSs and associated MUs. Here, the access links between MUs and their DBS are using RF communications, and the backhaul link between the DBS and its associated working MBS is applying FSO communications. Note that FSO communications is a point-to-point wireless communications technology that can achieve a very high throughput over a long distance [14, 65]. Applying FSO as the wireless backhaul communications can dramatically increase the network capacity, and significantly reduce the delay of transmitting data between MUs and working MBSs via DBSs [18].

## 4.1 FSO Communication Architecture

FSO communications has been proved to provision a high speed point-to-point communications [14] [65], and integrating drones into the FSO system has recently been explored. Fawaz *et al.* [21] proposed a drone-assisted FSO relay system, where a drone equipped with an FSO transceiver is considered as a relay node to relay the FSO beam between an FSO transmitter and an FSO receiver. The drone-assisted

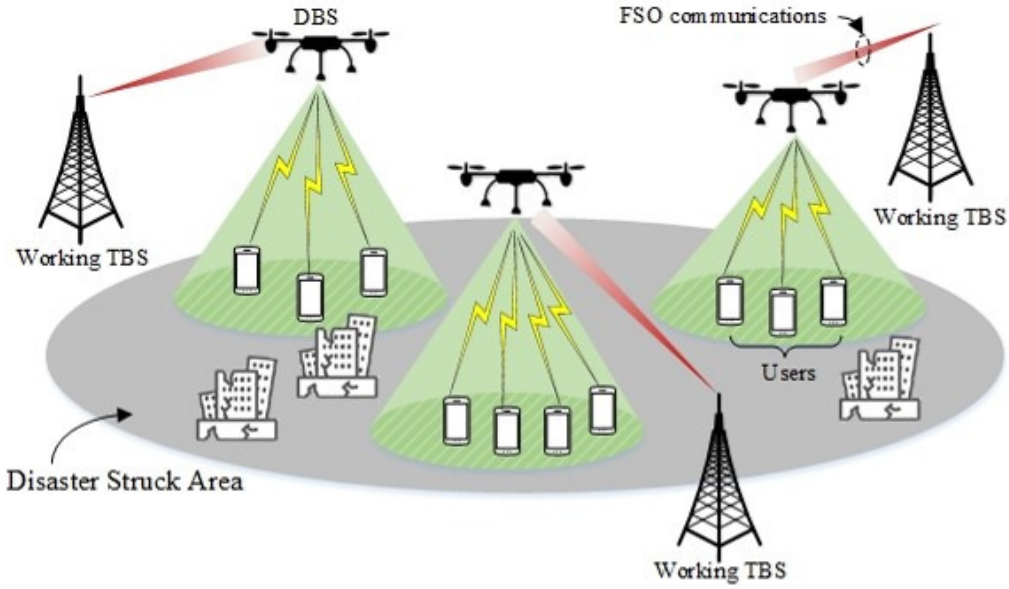


**Figure 4.1** FSO-based drone-assisted mobile access network architecture.

FSO relay system may reduce the atmosphere attenuation of the FSO link, especially when the distance between the FSO transmitter and the FSO receiver is very long. Applying FSO and drones as the front-hauling/back-hauling technology in mobile networks has recently been proposed [5], where geographically distributed base stations are connected to their nearby drones (which are hovering in the air) via FSO communications, and these drones cooperate with each other to establish an FSO-based drone ad-hoc network, which is to deliver the traffic between the mobile core network and distributed base stations. FSO communications between different drones is deployed in the drone ad-hoc network.

FSO communications has been proposed to be utilized in mobile networks; here, the placement of DBSs using FSO as the backhaul links between a DBS and its associated MBS in disaster-struck areas is the primary work. As mentioned before, using FSO communications and DBSs can quickly establish network connections to MUs in disaster-struck areas in carrying out emergency rescue.

### 4.1.1 RF access link model

The communications channel between an MU and its associated DBS is normally modeled as a probabilistic LoS channel. Denote the pathloss between DBS $i$ and MU $j$ (in dB) in LoS and NLoS as $\eta_{ij}^{LoS}$ and $\eta_{ij}^{NLoS}$ [3], respectively,

$$\eta_{ij}^{LoS} = 20\log\left(\frac{4\pi f_c d_{ij}}{c}\right) + \xi^{LoS}, \tag{4.1}$$

$$\eta_{ij}^{NLoS} = 20\log\left(\frac{4\pi f_c d_{ij}}{c}\right) + \xi^{NLoS}, \tag{4.2}$$

where $\xi^{LoS}$ and $\xi^{NLoS}$ stand for the average value of excessive pathloss in LoS and NLoS, respectively, $f_c$ is the carrier frequency, $c$ is the speed of light, and $d_{ij}$ is the distance between DBS $i$ and MU $j$. Excessive pathloss is the additional pathloss on top of the free space pathloss incurred between a DBS and an MU. As illustrated in Figure 4.2, $d_{ij}$ can be calculated by

$$d_{ij} = \sqrt{(x_i^d - x_j)^2 + (y_i^d - y_j)^2 + h^2(x_i^d, y_i^d)}. \tag{4.3}$$

Here, $h\left(x_i^d, y_i^d\right)$ is the altitude of DBS $i$ when DBS $i$ is deployed at the horizontal location $\left\langle x_i^d, y_i^d \right\rangle$, and $\langle x_j, y_j \rangle$ indicates the horizontal location of MU $j$. The horizontal distance between MU $j$ and DBS $i$ is denoted by $l_{ij}$

$$l_{ij} = \sqrt{(x_i^d - x_j)^2 + (y_i^d - y_j)^2}. \tag{4.4}$$

The probability of having LoS between DBS $i$ and MU $j$ ($\rho_{ij}$) is

$$\rho_{ij} = \frac{1}{1 + be^{-\beta(\theta_{ij} - b)}}, \tag{4.5}$$

where $b$ and $\beta$ are the two environmental parameters in the disaster-struck area, and $\theta_{ij}$ is the elevation angle between DBS $i$ and MU $j$ (as indicated in Figure 4.2), i.e.,

$$\theta_{ij} = \arcsin\left(\frac{h\left(x_i^d, y_i^d\right)}{d_{ij}}\right). \tag{4.6}$$

Based on Equations (4.5) and (4.6), DBS $i$ at a higher altitude leads to a larger value of elevation angle and incurs a higher probability of having an LoS link to MU $j$.

The average pathloss between DBS $i$ and MU $j$, denoted as $\bar{\eta}_{ij}$, can be modeled as [31]

$$\bar{\eta}_{ij} = \rho_{ij}\eta_{ij}^{LoS} + (1-\rho_{ij})\eta_{ij}^{NLoS}. \tag{4.7}$$

Note that DBS $i$ can communicate with MU $j$ if the average pathloss between MU $j$ and DBS $i$ is smaller than a predefined threshold $\eta^{th}$. Thus, the horizontal distance between DBS $i$ and MU $j$ is maximized when

$$\bar{\eta}_{ij} = \eta^{th}. \tag{4.8}$$

**Definition 1** ***The optimal elevation angle between DBS*** *$i$* ***and MU*** *$j$ is defined as the elevation angle between DBS $i$ and MU $j$ that maximizes the horizontal distance between DBS $i$ and MU $j$.*

In order to find the optimal elevation angle (denoted as $\theta_{ij}^*$), the derivative of $\eta^{th}$ is taken with respect to $\theta_{ij}$. By letting $\frac{\partial l_{ij}}{\partial \theta_{ij}} = 0$, $\theta_{ij}^*$ is acquired by:

$$\frac{\pi}{9\ln(10)}\tan\theta_{ij}^* + \frac{b\beta\left(\eta_{ij}^{LoS}+\eta_{ij}^{NLoS}\right)e^{\left(-\beta\left(\theta_{ij}^*-b\right)\right)}}{\left(be^{\left(-\beta\left(\theta_{ij}^*-b\right)\right)}+1\right)^2} = 0 \tag{4.9}$$

By substituting $\theta_{ij} = \theta_{ij}^*$ into Equation (4.8), the related maximum horizontal distance between DBS $i$ and MU $j$, denoted as $l_{ij}^{max}$, is derived. The altitude of DBS $i$ with the largest coverage ($h_{ij}^*$) is

$$h_{ij}^* = l_{ij}^{max}\tan\theta_{ij}^*. \tag{4.10}$$

### 4.1.2 Data rate model of wireless access link

As mentioned earlier, multiple DBSs are deployed in the disaster-struck area. Each DBS is associated with its nearby working MBS, and the DBS can download traffic

from that MBS and forward them to MUs. Different DBSs use different spectrum bands to relay traffic to their MUs, and MUs in downloading traffic from their DBSs do not interfere with each other. Denote $B_i$ as the total available bandwidth for DBS $i$ in transmitting traffic to associated MUs, and $b_{ij}$ is used to represent the amount of bandwidth allocated for MU $j$ in downloading traffic from DBS $i$. We can calculate the data rate of MU $j$ in downloading traffic from DBS $i$ (denoted as $r_{ij}$) as

$$r_{ij} = b_{ij} \log \left(1 + \frac{P_i 10^{-\bar{\eta}_{ij}/10}}{N_0}\right), \tag{4.11}$$

where $P_i$ indicates the transmission power of DBS $i$. The downlink scenario is considered in this work because the downlink traffic is much heavier than the uplink traffic (note that the ratio of downlink to uplink traffic is 6:1 [20]).

### 4.1.3 FSO communication model

Denote $\boldsymbol{I}$ as the set of DBSs being deployed in the disaster-struck area, and $i \in I$ is used to index these DBSs. Denote $\boldsymbol{J}$ as the set of MUs in the disaster-struck area, and $j \in J$ is used to index these MUs. Let $a_{ij}$ be the binary variable to indicate whether MU $j$ is served by DBS $i$ (i.e., $a_{ij} = 1$) or not (i.e., $a_{ij} = 0$).

FSO communications is applied to enable DBSs in downloading traffic from nearby MBSs, as shown in Figure 4.2. The data rate model of the FSO link between DBS $i$ and its MBS can be modeled as [5]

$$R_i = \frac{P_t}{E_p N_b} \frac{r_s^2}{\left(\theta_g d_i^F/2\right)^2} \eta_t \eta_r 10^{-e^{\sigma d_i^F}}, \tag{4.12}$$

where $N_b$ is the sensitivity of the receiver (photons/bit); $E_p$ is the energy of each photon, i.e., $E_p = h_p c/\lambda$ (here, $h_p$ is the Planck's constant, $c$ is the light speed, and $r_s$ is the radius of the FSO beam at the DBS $i$'s associated MBS); $\theta_g$ is the divergence angle of the optical beam; $\eta_t$ is the coefficient for converting electrical energy into optical energy at the DBS $i$'s associated MBS; $\eta_r$ is the coefficient for converting

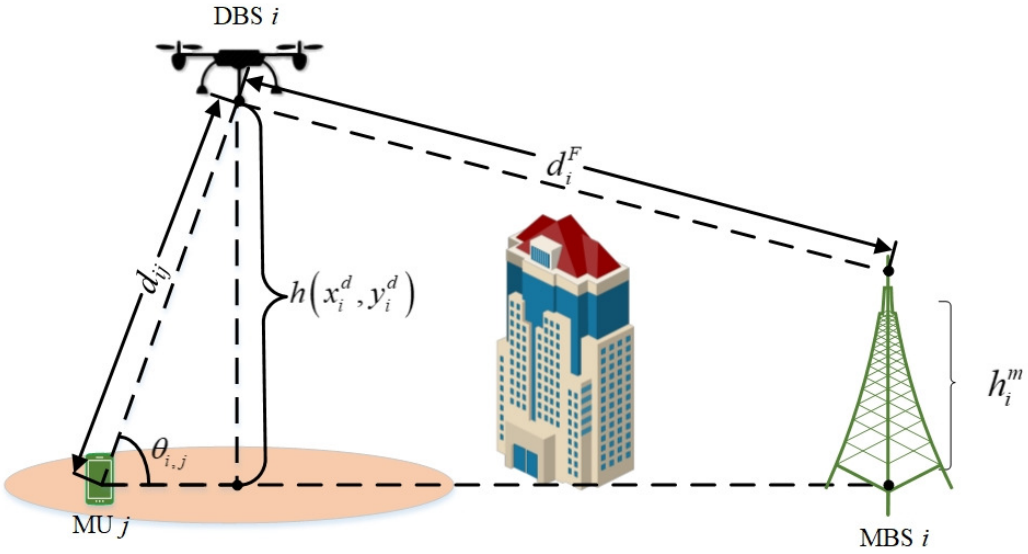


**Figure 4.2** Pathloss model.

optical energy into electrical energy at DBS $i$ ; $d_i^F$ is the distance between DBS $i$ and its associated MBS, i.e.,

$$d_i^F = \sqrt{(h(x_i^d, y_i^d) - h_i^m)^2 + (x_i^d - x_i^m)^2 + (y_i^d - y_i^m)}, \tag{4.13}$$

where $\langle x_i^m, y_i^m, h_i^m \rangle$ indicates the 3-D location of DBS $i$'s associated MBS; $\sigma$ in Equation (4.12) is the atmospheric attenuation coefficient, given by [51] as

$$\sigma = \frac{3.91}{v} \left( \frac{\lambda}{550} \right)^{-q} \tag{4.14}$$

where $v$ is the visibility (the maximum distance that one object can be clearly discerned). Denote $q$ as the size distribution of the scattering particles. The relationship between $q$ and $v$ is given by [51]

$$q = \begin{cases} 1.6, & v > 50, \\ 1.3, & 6 < v \leq 50, \\ 0.16v + 0.34, & 1 < v \leq 6, \\ v - 0.5, & 0.5 < v \leq 1, \\ 0, & v, \leq 0.5, \end{cases} \tag{4.15}$$

where the value of $v$ depends on the weather conditions. For example, $v > 50$ when the weather reflects a clear sky, $1 < v \leq 6$ for a hazy weather, and $v \leq 1$ for foggy weather.

### 4.1.4 QoS aware DBS placement strategy

Assume that the number of available DBSs is predetermined. These DBSs can be deployed to help the MUs in the disaster-struck area download data from their associated MBSs. Assuming that each MBS is only equipped with one FSO transceiver, i.e., one MBS can only communicate with one DBS. Denote $a_{ij}$ as the binary variable to indicate whether MU $j$ is associated with DBS $i$ (i.e., $a_{ij} = 1$) or not (i.e., $a_{ij} = 0$). The DBS configuration and MUs association problem is formulated as determining the 3-D locations of DBSs, MUs association, as well as the bandwidth allocation to different MUs in order to maximize the number of satisfied MUs. In the disaster-struck area, the mobile network infrastructure may be damaged, and MUs in the area are unable to communicate with others, such as the first response team and their families. Establishing emergence communications is very critical for MUs in the disaster-struck area. For example, reporting the locations of MUs (by sending short messages) to the first response team can facilitate the rescue. Here, sending short messages does not require a high data rate. Thus, enabling more MUs to be able to communicate with the first response team is considered as the ultimate objective,

(i.e., their QoS in terms of data rate requirements is met). That is,

$$\mathbf{P0:} \underset{x_i^d, y_i^d, h(x_i^d, y_i^d), a_{ij}}{\arg\max} \sum_{i \in \boldsymbol{I}} \sum_{j \in \boldsymbol{J}} a_{ij}, \tag{4.16}$$

$$s.t.: C1: \sum_{i \in \boldsymbol{I}} a_{ij} \leq 1, \ \forall j \in \boldsymbol{J}, \tag{4.17}$$

$$C2: f^{min}(x_i^d, y_i^d) \leq h(x_i^d, y_i^d) \leq f^{max}(x_i^d, y_i^d), \tag{4.18}$$

$$C3: a_{ij}(\eta_{ij} - \eta_{ij}^{th}) \leq 0, \ \forall j \in \boldsymbol{J}, \ \forall i \in \boldsymbol{I}, \tag{4.19}$$

$$C4: a_{ij}(r_{ij} - r_j^{th}) \geq 0, \ \forall i \in \boldsymbol{I}, \forall j \in \boldsymbol{J}, \tag{4.20}$$

$$C5: \sum_{j \in \boldsymbol{J}} a_{ij} r_{ij} \leq R_i, \ \forall i \in \boldsymbol{I}, \tag{4.21}$$

$$C6: \sum_{j \in \boldsymbol{J}} a_{ij} b_{ij} \leq B_i, \ \forall i \in \boldsymbol{I}, \tag{4.22}$$

where Constraint C1 ensures that each MU is served by at most one DBS; Constraint C2 imposes the altitude constraints of deploying a DBS, where $f^{min}(x_i^d, y_i^d)$ implies the minimum altitude of DBS $i$ to maintain the LoS between DBS $i$ and its associated MBS, if DBS $i$ is deployed at $\langle x_i^d, y_i^d \rangle$, and $f^{max}(x_i^d, y_i^d)$ is the maximum altitude that DBS $i$ can reach. Constraint C3 indicates that MU $j$ can be associated with DBS $i$ (i.e., $a_{ij} = 1$) if the pathloss between MU $j$ and DBS $i$ is not larger than the threshold $\eta^{th}$ (i.e., $\eta_{ij} - \eta^{th} \leq 0$). Constraint C4 implies that QoS in terms of the data rate requirement of MU $j$ (denoted as $r_j^{th}$) should be satisfied if it is associated with DBS $i$; Constraint C5 implies that the data rate of the backhaul link between DBS $i$ and its associated MBS should be no less than the data rate of the access link for DBS $i$ (which is equal to the sum of all the data rates of the MUs associated with DBS $i$). Essentially, Constraint C5 ensures that the backhaul link is not the bottleneck. Constraint C6 ensures the total bandwidth allocated to MUs by each DBS is within the total bandwidth it can use.

A heuristic algorithm, i.e., QoS awaRe dronE base Station plaCement and mobile User association stratEgy (RESCUE), is proposed to efficiently solve **P0**.

**Table 4.1** List of Notations

| | |
|---|---|
| $\boldsymbol{I}$ | Set of all available DBSs |
| $\boldsymbol{J}$ | Set of all MUs |
| $i$ | Index of DBSs ($i \in \boldsymbol{I}$) |
| $j$ | Index of MUs ($j \in \boldsymbol{J}$) |
| $a_{ij}$ | Binary variable to indicate the user association |
| $x_i^d$, $y_i^d$ | Horizontal location of DBS $i$ |
| $x_i^m$, $y_i^m$ | Horizontal location of DBS $i$'s associated MBS |
| $x_j$, $y_j$ | Horizontal location of MU $j$ |
| $d_{ij}$ | Horizontal distance between DBS $i$ and MU $j$ |
| $h(x_i^d, y_i^d)$ | Altitude of DBS $i$ if DBS $i$ is over location ($x_i^d$, $y_i^d$) |
| $f^{max}(x_i^d, y_i^d)$ | Maximum altitude of a DBS at location $(x_i^d, y_i^d)$ |
| $f^{min}(x_i^d, y_i^d)$ | Minimum altitude of a DBS at location $(x_i^d, y_i^d)$ |
| $\eta_{ij}$ | Average pathloss between DBS $i$ and MU $j$ |
| $\eta^{th}$ | Average pathloss threshold |
| $h_i^m$ | Altitude of MBS $i$ |
| $r_{ij}$ | Downloading data rate from DBS $i$ to MU $j$ |
| $r_j^{th}$ | Downloading data rate requirement of MU $j$ |

The basic idea of RESCUE is to decompose **P0** into two sub-problems, i.e., DBS placement and bandwidth allocation. By solving the two sub-problems iteratively, RESCUE can achieve a near optimal solution of **P0**. RESCUE is summarized in Algorithm 2. **Initial 3-D DBS placement**: The disaster-struck area is first divided into a number of locations with the same size. Denote the set of these locations as $N$. So, if DBS $i$ is placed over location $n$ (where $n \in N$), then the 2-D coordinate of DBS $i$ (i.e., $\langle x_i^d, y_i^d \rangle$) equals to the center of location $n$, and DBS $i$ can connect to its associated MBS to download traffic. The objective of the initial 3-D DBS placement is to find the optimal location where DBS $i$ can cover the maximum number of MUs (which are not associated with other deployed DBSs). Note that an MU is covered by a DBS implies that the pathloss between the MU and the DBS is no larger than the pathloss threshold $\eta^{th}$. Denote $\boldsymbol{J'}$ as the set of MUs that are not associated with any deployed DBSs (i.e., $\boldsymbol{J'} = \{j \in \boldsymbol{J} | a_{ij} = 0, \forall i \in \boldsymbol{I}.\}$), and $\boldsymbol{J'} = \boldsymbol{J}$ when the first DBS is placed. In order to find the optimal location with respective to DBS $i$, the controller will iteratively place DBS $i$ over each location in the disaster-struck area and select the one which can cover the maximum number of MUs.

DBS $i$ is placed over location $n$ if location $n$ is selected. The altitude of DBS $i$ with the largest coverage area can be obtained by Equation (4.10), i.e., $h(x_i^d, y_i^d) = h_i^*$. Note that, in order to satisfy C2 in **P0**, $h(x_i^d, y_i^d) = f^{min}(x_i^d, y_i^d)$ if $h_i^* < f^{min}(x_i^d, y_i^d)$ and $h(x_i^d, y_i^d) = f^{max}(x_i^d, y_i^d)$ if $h_i^* > f^{max}(x_i^d, y_i^d)$.

After having determined the altitude of DBS $i$ at location $n$, the average pathloss between DBS $i$ and all the MUs in $\boldsymbol{J'}$ is calculated. The controller will check if these MUs can be covered by DBS $i$ or not. Denote $\boldsymbol{K}_{in}$ as the set of MUs that can be covered by DBS $i$ deployed over location $n$, i.e., $\boldsymbol{K}_{in} = \{j \in J' | \bar{\eta}_{ij} \leq \eta^{th}.\}$, and $|\boldsymbol{K}_{in}|$ is used to indicate the number of MUs covered by DBS $i$. Thus, the optimal location of DBS $i$ is the location that incurs the largest value of $|\boldsymbol{K}_{in}|$, i.e.,

$n_i^* = \arg\max\{|\boldsymbol{K}_{in}||n \in N.\}$. Therefore, DBS $i$ will be placed over the center of location $n^*$.

**Bandwidth allocation and MU association**: After having determined the 2-D location of DBS $i$, each MU covered by DBS $i$ should be allocated sufficient bandwidth to satisfy its data rate requirement (i.e., C4 in **P0**). Here, the bandwidth requirement of MU $j$ is defined as the minimum amount of bandwidth that meets the data rate requirement of MU $j$, i.e.,

$$b_{ij} = \frac{r_{ij}}{\log\left(1 + \frac{P_i 10^{-\bar{\eta}_{ij}/10}}{N_0}\right)}. \tag{4.23}$$

However, the total amount of available bandwidth of DBS $i$ (i.e., $B_i$) is limited, and so not all the MUs covered by DBS $i$ can be allocated sufficient bandwidth to meet their data rate requirements. In order to maximize the number of the MUs (such that their data rate requirements are met), DBS $i$ will first allocate bandwidth to the MU, which incurs the least bandwidth requirement. The required bandwidth is calculated by the pathloss between MU and DBS $i$ and the required data rate.

We construct an array by sorting all the MUs covered by DBS $i$ (i.e., $\forall j \in \boldsymbol{K}_{in^*}$) in ascending order according to their bandwidth requirements ($b_{ij}$). Assume that MU $j'$ is the first MU in the array. Then, we allocate $b_{ij'}$ amount of bandwidth to MU $j'$, associate MU $j'$ to DBS $i$, i.e., $a_{ij'} = 1$, and update the available bandwidth of DBS $i$ by $B_i = B_i - b_{ij'}$.

We then select the next MU in the array, allocate the required bandwidth to the MU, and associate the MU to DBS $i$. The iteration continues until all the MUs covered by DBS $i$ are associated to DBS $i$ (i.e., $\forall j \in \boldsymbol{K}_{in^*}, a_{ij} = 1$), or DBS $i$ does not have enough bandwidth to meet the bandwidth requirement of the selected MU, or the overall data rate between the associated MUs and DBS $i$ exceeds the capacity of the FSO backhaul link between DBS $i$ and its associated MBS (i.e., C5 in **P0**).

**Altitude adjustment**: when unable to meet the data rate requirements of some MUs covered by DBS $i$ because of the limited available bandwidth of DBS $i$ (i.e., $B_i$), the altitude of DBS $i$ will be adjusted to meet more MUs' data rate requirements.

We denote $h_i^*$ as the altitude of DBS $i$ obtained from the **initial 3-D DBS placement**, and $\delta$ as the step size of adjusting the value of $h_i^*$, where $\delta^{\min} \leq \delta \leq \delta^{\max}$. Here, $\delta^{\min}$ and $\delta^{\max}$ are the minimum and maximum step size of $\delta$, respectively. Initially, $\delta = \delta^{\min}$.

We generate two temporary altitudes of DBS $i$ ($h_i^-$ and $h_i^+$) for further adjustment, i.e., $h_i^- = \max\left(h_i^* - \delta, f^{min}(x_i^d, y_i^d)\right)$ and $h_i^+ = \min\left(h_i^* + \delta, f^{max}(x_i^d, y_i^d)\right)$, respectively. The number of MUs associated to DBS $i$ (i.e., $\sum_{j \in \boldsymbol{J'}} a_{ij}$ ) is calculated by re-executing **bandwidth allocation and MU association** based on the two temporary altitudes of DBS $i$ (i.e., $h_i^-$ and $h_i^+$), respectively.

Let $m(h_i^*)$, $m(h_i^+)$, and $m(h_i^-)$ be the number of the associated MUs when the altitude of DBS $i$ is $h_i^*$, $h_i^+$, and $h_i^-$, respectively. Here, if the adjusted altitude of DBS $i$ does not increase the number of associated MUs, then the original altitude of DBS $i$ is kept, i.e.,

$$h_i^* = h_i^*, \text{if } \mathrm{m(h_i^*)} \geq \mathrm{m(h_i^+)} \ \& \ \mathrm{m(h_i^*)} \geq \mathrm{m(h_i^-)},$$

and the step size is adjusted as $\delta = \delta + \delta^{\min}$. If the adjusted altitude of DBS $i$ increases the number of the associated MUs, then the altitude of DBS $i$ is updated as

$$h_i^* = \begin{cases} h_i^+, \text{if } \mathrm{m}\left(\mathrm{h_i^+}\right) > \mathrm{m}\left(\mathrm{h_i^*}\right) \ \& \ \mathrm{m}\left(\mathrm{h_i^+}\right) \geq \mathrm{m}\left(\mathrm{h_i^-}\right), \\ h_i^-, \text{if } \mathrm{m}\left(\mathrm{h_i^-}\right) > \mathrm{m}\left(\mathrm{h_i^*}\right) \ \& \ \mathrm{m}\left(\mathrm{h_i^-}\right) > \mathrm{m}\left(\mathrm{h_i^+}\right), \end{cases} \tag{4.24}$$

and $\delta = \delta^{\min}$.

Then, the controller will keep adjusting the altitudes of DBS $i$ by going back to Step 2) in **altitude adjustment**. The altitude adjustment continues until $\delta > \delta^{\max}$.

Note that the RESCUE algorithm is periodically executed to update the DBS placement, bandwidth allocation, and MU association in order to accommodate the MU mobility.

The RESCUE algorithm comprises three processes, i.e., deriving the optimal 2-D location, altitude, and MU association and bandwidth allocation for all the DBSs. The time complexity of deriving the optimal 2-D location of a DBS (i.e., Steps 3-8 in Algorithm 1) is $O(|N||J|)$ (where $|N|$ and $|J|$ are the numbers of locations and MUs in the disaster-struck area, respectively). The time complexity of deriving the altitude and MU association of a DBS (i.e., Steps 9-22 in Algorithm 1) is $O(|\boldsymbol{J}| + \frac{h^{\max}-h^{\min}}{\delta^{\min}})$ (where $h^{\max}$ and $h^{\min}$ are the highest and lowest altitude of the DBS for all locations, respectively). Therefore, the time complexity of RESCUE is $O(|\boldsymbol{I}|(|N||\boldsymbol{J}| + |\boldsymbol{J}| + \frac{h^{\max}-h^{\min}}{\delta^{\min}})) = O(|\boldsymbol{I}||N||\boldsymbol{J}| + |\boldsymbol{I}|\frac{h^{\max}-h^{\min}}{\delta^{\min}})$ (where $|\boldsymbol{I}|$ is the number of DBSs).

The space complexity (i.e., the required memory space) of RESCUE is determined by the required memory for storing the MU movement matrix (which indicates the locations of all MUs in different time slots) and MU information matrix (which imposes the data rate requirements of the MUs). The space complexity of the MU movement and that of the MU information matrix are $O(|\boldsymbol{I}||N|)$ and $O(|\boldsymbol{J}|)$, respectively. Thus, the space complexity of RESCUE is $O(|\boldsymbol{I}||N| + |\boldsymbol{J}|)$.

**Algorithm 2** RESCUE

1: Repeat for all DBS $i \in \boldsymbol{I}$

2: **for** each location $n \in N$ **do**

3: Place DBS $i$ over location $n$.

4: Calculate the altitude of DBS $i$ with the largest coverage over location $n$, denoted as $h_n$, based on $f^{max}(x_i^d, y_i^d)$, $f^{max}(x_i^d, y_i^d)$.

5: Calculate the number of MUs covered by DBS $i$, i.e., $|\boldsymbol{K}_{in}|$.

6: **end for**

7: Calculate the optimal location for DBS $i$, i.e., $n^*$, where $n_i^* = \arg\max\{|K_{in}| \, | n \in N\}$.

Denote $h_i^*$ as the altitude of DBS $i$ with the largest coverage, when it is deployed over location $n^*$.

8: Construct an array by sorting all the MUs covered by DBS $i$ in ascending order according to their bandwidth requirements $b_{ij}$ (where $\forall j \in \boldsymbol{K}_{in^*}$).

9: Iteratively select and allocate bandwidth to the MU that within the coverage of DBS $i$ and update the available bandwidth of DBS $i$.

10: Initialize the step size $\delta = \delta^{min}$.

11: **while** $\delta \leq \delta^{max}$ **do**

12: $h_i^- = \max\left(h_i^* - \delta, f^{min}(x_i^d, y_i^d)\right)$.

13: $h_i^+ = \min\left(h_i^* + \delta, f^{max}(x_i^d, y_i^d)\right)$.

14: Execute bandwidth allocation and MU association with the altitude of DBS $i$ being $h_i^*$, $h_i^-$ and $h_i^+$, respectively.

15: Calculate $m(h_i^*)$, $m(h_i^+)$, and $m(h_i^-)$.

16: **if** $m(h_i^*) > m(h_i^+)$ and $m(h_i^*) > m(h_i^-)$ **then**

17: $\delta = \delta + \delta^{\min}$.

18: **else**

19: Update $h_i^*$ based on Eq. (4.24).

20: **end if**

21: **end while**

### 4.1.5 Simulation results

In order to validate the performance of RESCUE, extensive simulations have been conducted to compare the performance of RESCUE with two other baseline algorithms, i.e., traffic load aware DBS configuration (TLA) [10] and pathloss aware DBS configuration (PLA) [16]. The basic idea of TLA is to maximize the overall data rate between DBSs and MUs by first allocating bandwidth to the MUs with lower pathloss to their associated DBSs. However, TLA does not yield the optimal DBS deployment, and the locations of DBSs, derived from RESCUE, will be applied to

TLA. That is, TLA and RESCUE have the same DBS deployment but apply different access link bandwidth allocation methods. The basic idea of PLA is to jointly optimize the bandwidth allocation and horizontal locations of DBSs in order to minimize the average pathloss between MUs and their associated DBSs. However, the altitudes of DBSs are fixed and predefined. Here, assuming that if PLA determines to deploy DBS $i$ over location $(x_i^d, y_i^d)$, then the altitude of the DBS is the minimum altitude to achieve LoS between the drone and its working base station, i.e., $f^{min}(x_i^d, y_i^d)$.

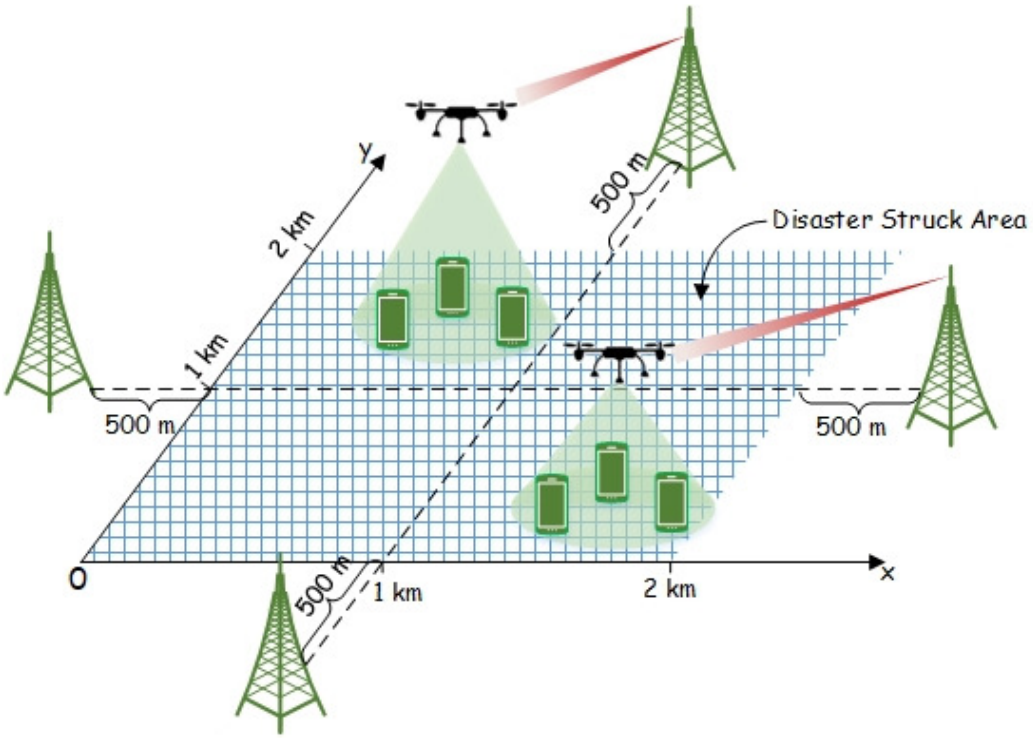


**Figure 4.3** Simulation setups.

The simulation is set up as follows: the size of the disaster-struck area is $2 \times 2$ $km$. The disaster-struck area is further divided into $100 \times 100$ small locations with the same size of $20 \times 20$ $m$. There are 4 working MBSs around the disaster-struck area. The locations of these working MBSs are depicted in Figure 4.3. The distribution of MUs in the disaster-struck area follows a 2-D Poisson distribution with the average MU density equal to 5 MUs/location. The pathloss requirements of all MUs are the

**Table 4.2** Simulation Parameters II

| | |
|---|---|
| FSO transmission power ($P_t$) | 200 $mWatt$ |
| Divergence angle ($\theta_g$) | 1 $mrad$ |
| Receiver radius ($r$) | 0.05 $m$ |
| Receiver sensitivity ($N_b$) | 100 $photons/bit$ |
| FSO wavelength ($\lambda$) | 1550 $nm$ |
| Visible distance $v$ | 10 $km$ |
| Available MBS/DBS | 4 |
| Disaster area radius | 2 $km$ |
| Maximum altitude of DBS ($f^{max}$) | 200 $m$ |
| Carrier frequency ($f_c$) | 2 $GHz$ |
| Environment index ($b$) | 9.61 [49] |
| Environment index ($\beta$) | 0.16 [49] |
| Average excessive pathloss in LoS ($\xi^{LoS}$) | 1 $dB$ |
| Average excessive pathloss in NLoS ($\xi^{NLoS}$) | 20 $dB$ |
| Noise power spectral density ($N_0$) | -104 $dBm/Hz$ |
| DBS downlink transmission power | 20 $dBm$ |
| Available bandwidth for each DBS ($B_i$) | 5 $MHz$ |

same, i.e., $\eta^{th} = 110\ dB$. Also, the data rate requirements of MUs are generated based on the normal distribution with the mean and standard deviation equal to 0.3 Mbps and 0.1 Mbps, respectively. Other simulation parameters are shown in Table 4.2.

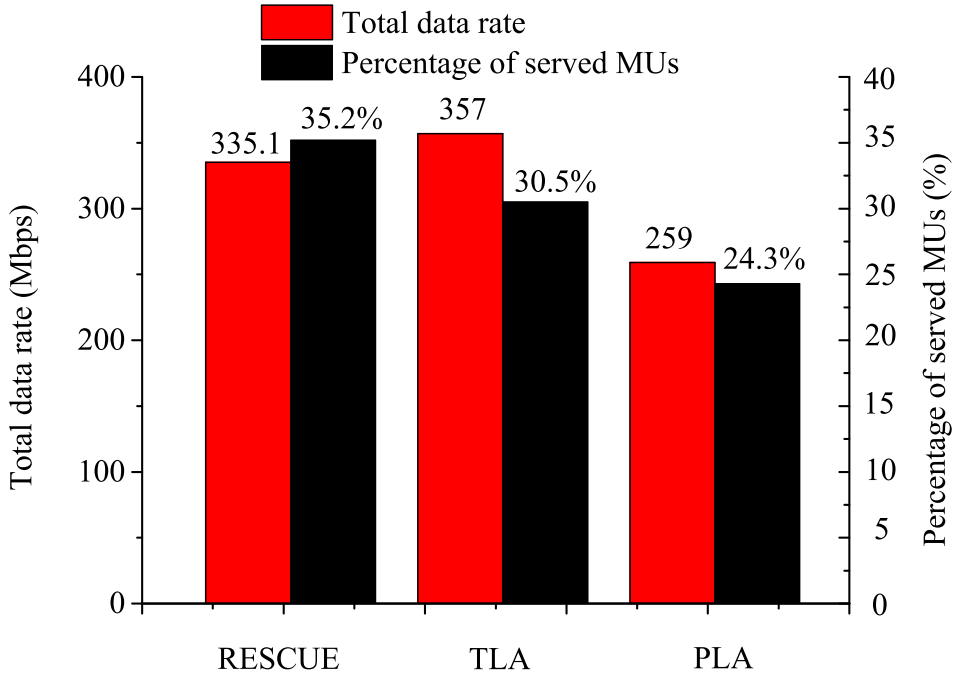


**Figure 4.4** Fraction of served MUs and total data rate by different methods.

The total data rate (i.e., the aggregated data rate of all MUs) and the fraction of served MUs incurred by the three algorithms are shown in Figure 4.4. Here, the fraction of served MUs equals to the number of MUs with satisfied data rate requirements, divided by the total number of MUs in the disaster-struck area. The figure shows that RESCUE achieves the highest fraction of served MUs as compared to TLA and PLA; however, the total data rate incurred by RESCUE is lower than that incurred by TLA because RESCUE tries to maximize the number of served MUs, and so it prefers to allocate bandwidth to MUs, which require less bandwidth to meet their data rate requirements. On the other hand, TLA tries to maximize the overall

data rate of MUs, and so it prefers to allocate bandwidth to MUs, which have the lower pathloss to their DBSs. Also, PLA incurs the worst performance in terms of the total date rate and the fraction of served MUs because PLA does not optimize the altitude of DBSs and thus degrades its performance accordingly.

The cumulative distribution of served MUs' data rate requirements for the three methods is shown in Figure 4.5; RESCUE has more than 60% of served MUs with data rate requirements no larger than 2.75 *Mbps*; however, TLA only has less than 30% of served MUs with data rate requirements no larger than 2.75 *Mbps*. The result demonstrates that RESCUE prefers to allocate bandwidth to the MUs which require less bandwidth to meet their data rate requirements.

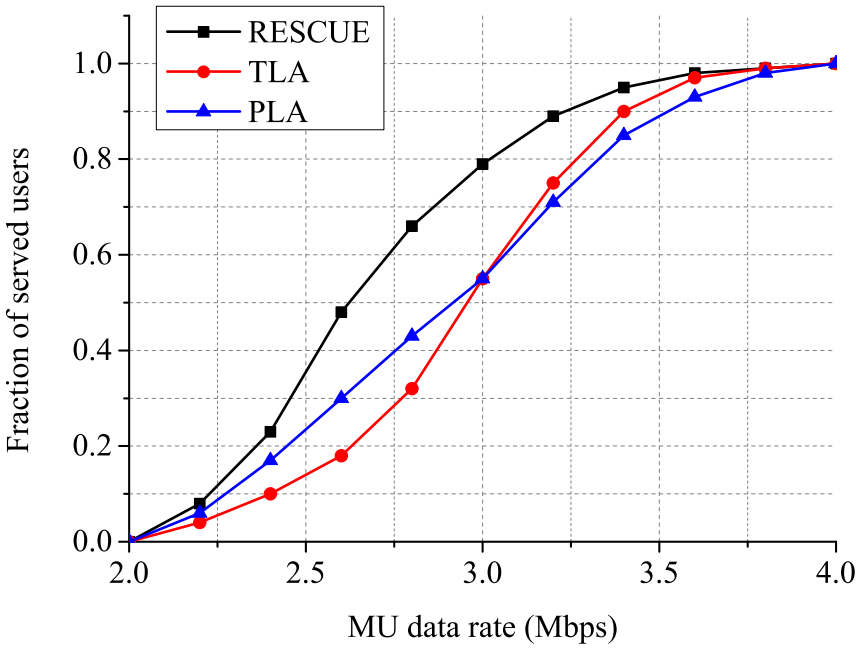


**Figure 4.5** Cumulative distribution of MUs with varying data rate requirement.

The fraction of served MUs and the total date rate by varying the average MU density of the area are shown in Figures 4.6 and 4.7, respectively. RESCUE always incurs the highest fraction of served MUs, and TLA always incurs the highest total

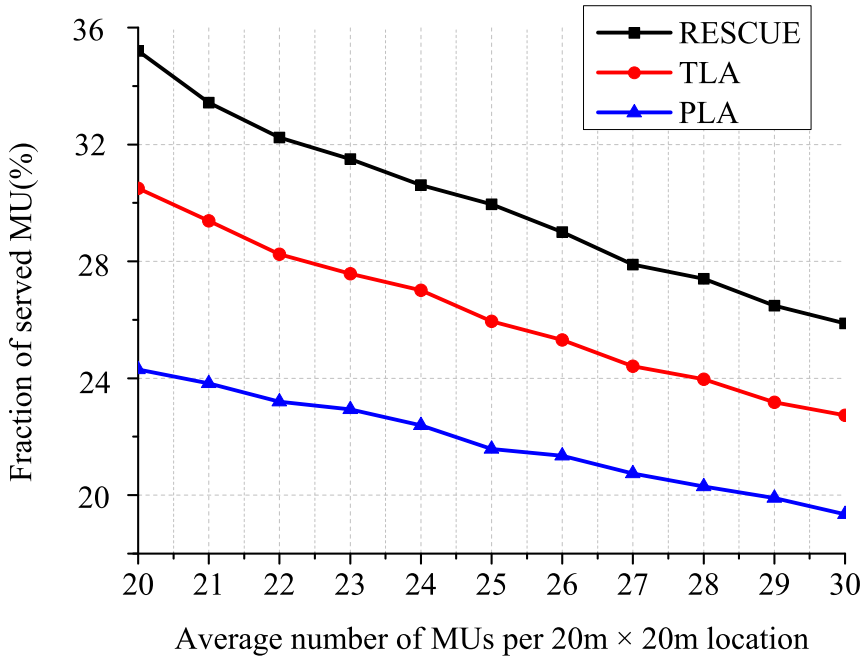


**Figure 4.6** Fraction of served MUs' data rate requirements.

data rate of MUs. However, as the average MU density of the area increases, the difference of the total data rate incurred by RESCUE and TLA diminishes.

The influence from the number of available DBSs to the network performance is investigated in follwing simulations. Note that the total amount of bandwidth assigned to these DBSs are fixed, and so having more available DBSs translates into less amount of bandwidth assigned to each DBS. The total data rate and the fraction of served MUs by varying the number of available DBSs are shown in Figures 4.8 and 4.9, respectively. Still, RESCUE achieves the highest fraction of served MUs and TLA achieves the highest total data rate. Meanwhile, the difference between the total data rate incurred by RESCUE and the one incurred by TLA reduces because as the number of deployed DBSs increases, the average pathloss between a DBS and an MU reduces, and so the MUs which are served by RESCUE (to allocate bandwidth in order to meet their data rate requirements) have the higher probability of having

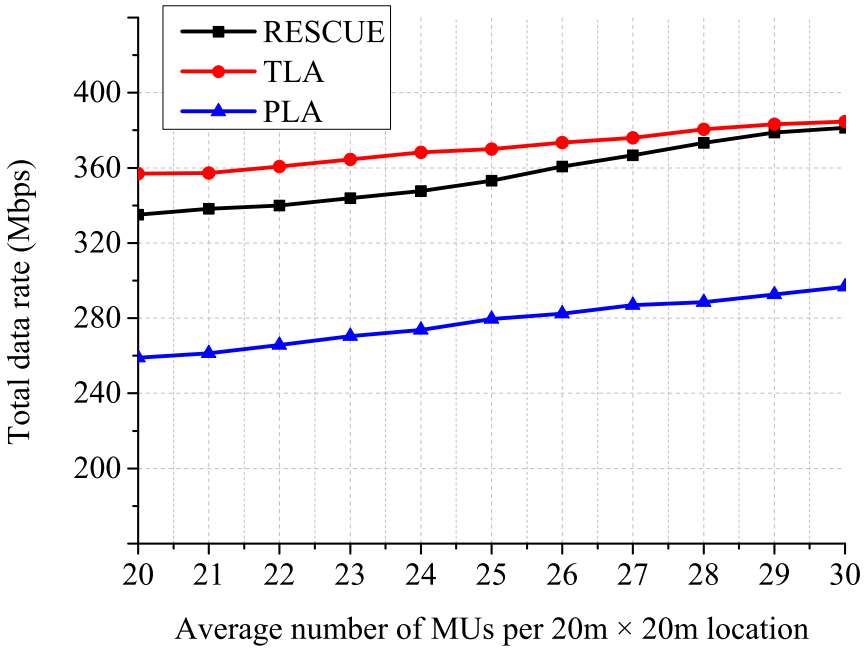


**Figure 4.7** Total data rate over different MU density.

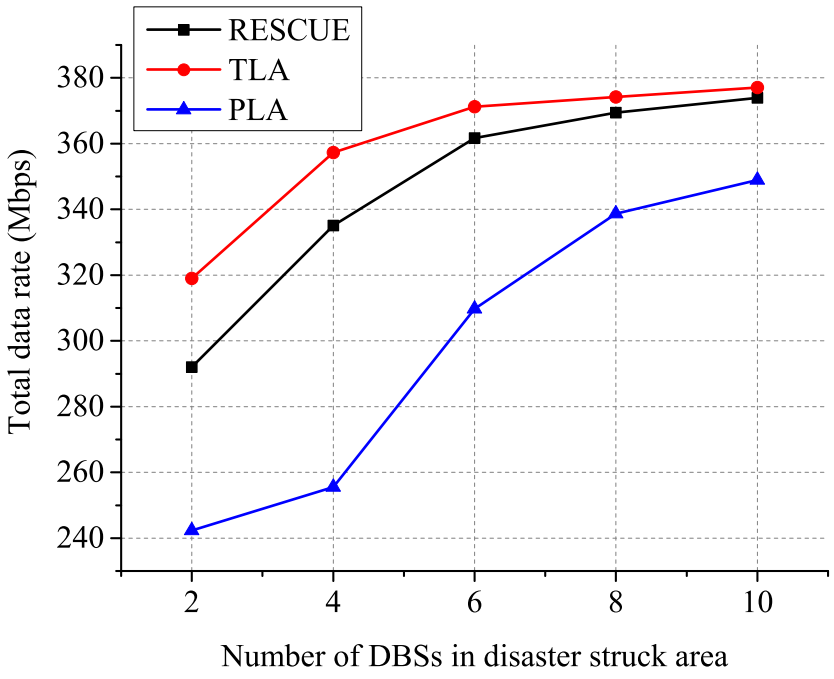


**Figure 4.8** Total data rate over different number of DBSs.

lower pathloss to their DBSs. That is, the MUs selected by RESCUE have a higher probability of also being selected by TLA as the number of deployed DBSs increases. In addition, the performance of PLA is still the worst since it does not optimize the altitude of DBSs, thus PLA incurs in a higher pathloss between MUs and their DBSs.

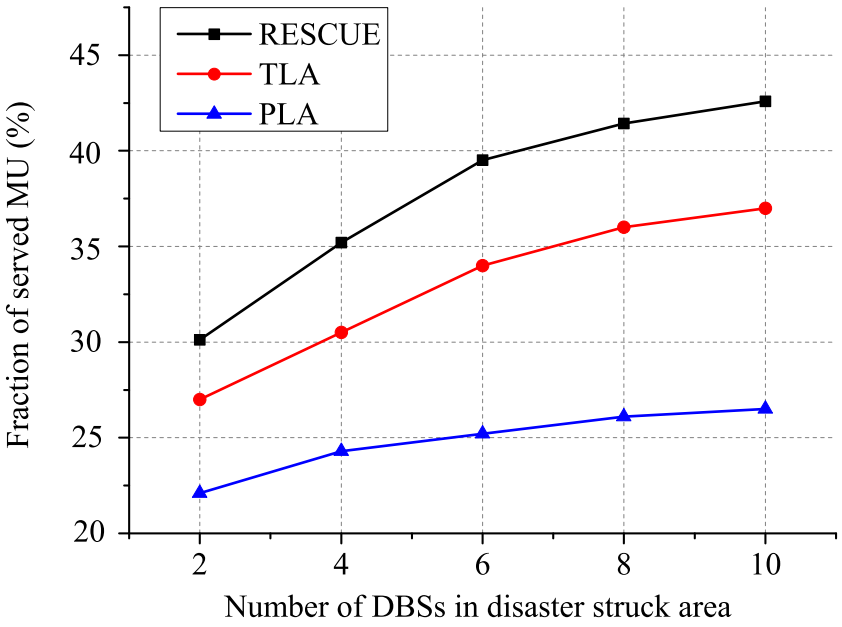


**Figure 4.9** Fraction of served MUs by varying number of DBSs.

## 4.2 FSO Charging

In order to extend the hovering time of DBS, a FSO charging system is proposed to argument the drone-assisted FSO backhaul system. Although a DBS can be quickly and efficiently placed over a disaster struck area (DSA) to set up emergency wireless communications, there are still some challenges. First, the DBS has to be placed over a DSA such that the distance between the DBS and the MUs in the DSA is close enough to achieve high access link data rates. However, in a large DSA, the DBS has to be deployed far away from the its associated working MBS, and the capacity of the backhaul link between the DBS and its associated MBS is limited. Accordingly,

a bottleneck may be generated on the backhaul link when the MUs download data from the working MBS via the DBS. Second, current commercial drones, which are normally powered by portable batteries, have the maximum flying time of around 30 minutes. That is, a DBS has to return to the control station for every 30 minutes of flight time to be charged for several hours. The limited flying time hinders the usage of applying drones in emergence communications. In order to significantly improve the backhaul link capacity while expanding the battery life of a drone, we propose to leverage free Space optics as backhaul and energizer for drone-assisted Networking (SoarNet) [7, 8] to provision emergency communications. As shown in Figure 4.10, an optical transmitter is embedded into an MBS and emits an optimal beam to a DBS. The emitted optical beam is used to transmit both data and energy to the DBS. An optical receiver is mounted on the DBS to receive the optical beam. The optical receiver is made up of two parts, i.e., a solar panel and an FSO receiver. The solar panel is used to obtain the optical energy to provide the DBS with extra energy in order to prolong its battery life. The FSO receiver is used to retrieve the data carried by the optical beam and transmit the received data to the MUs via the RF transmitter. Note that an FSO link has been demonstrated to provision a high link capacity over a long distance between two endpoints [65]. Meanwhile, it has been shown that optical beams, which are highly directional, can transmit/transfer energy more efficiently than traditional energy harvesting (such as RF and solar energy harvesting) [15]. Therefore, SoarNet can simultaneously transmit the data streams to the DBS at high speed and charge the DBS with high efficiency.

Many researchers have been explored the DBS placement and resource management methods in drone-assisted mobile networks. Yaliniz *et al.* [11] investigated a 3-D DBS deployment algorithm that can maximize the number of served MUs, where an MU is able to be served by a DBS only if the pathloss of the MU's access link can satisfy the requirements. In order to optimize the DBS deployment over a hotspot,

Sun and Ansari [55] designed a novel DBS placement and user association method that can maximize the spectrum efficiency of the hotspot. By placing several DBSs above a DSA, Wu *et al.* [59] proposed a cooperative DBS aided wireless network architecture, where DBS-to-DBS communications is used to balance the traffic load of different backhaul links. They designed a wireless channel assignment and multiple DBS deployment method to maximize the network throughput.

Applying FSO as the backhaul solution to improve the achievable data rate of the backhaul link in drone mobile networks has recently been proposed [64]. Sun *et al.* [56] designed a 3-D DBS deployment algorithm that maximizes the spectrum efficiency of the network, where the backhaul link is implemented as an FSO link. However, they assumed that the FSO-based backhaul link can provide sufficient link capacity to meet the data rate requirements from the access links between a DBS and the MUs. Fawaz *et al.* [21] applied a drone, which is equipped with an FSO transceiver, to relay traffic between, for example, two ground small cells, which do not satisfy the LoS criteria to maintain an FSO link. Alzenad *et al.* [5] explored an FSO-based vertical wireless communications architecture, where a number of drones (each is equipped with multiple FSO transceivers) are interconnected together to establish a drone relay network to relay traffic between geographically distributed MBSs and a gateway via FSO links. Based on the proposed FSO-based wireless communications architecture, Gu *et al.* [24] proposed a method to agilely alter the routing paths such that the overall throughput is maximized and total power consumption of the drones is minimized.

To extend the hovering time of drones, Alsharoa *et al.* [4] proposed that drones mounted with solar panels can collect solar energy, thus extending their hovering time. To avoid taking extra load for charging, Shin *et al.* [50] proposed to deploy movable wireless charging stations to charge drones. That is, movable wireless charging stations can be placed over drones to conduct wireless energy charging, and drones can

continuously provide service to MUs while charging. Sang-Won *et al.* [48] designed a two receiving coils charging station to increase the wireless charging efficiency. In comparison to the traditional RF wireless charge technologies, using optical wireless charging can achieve much higher efficiency [35]. Our previous works have designed and illustrated the SoarNet architecture to simultaneously transmit energy and data from an MBS to a DBS [8]. However, how to jointly optimize access link bandwidth assignment and the DBS deployment to maximize the hovering time of the DBS is still very challenging.

Based on the proposed architecture, a new DBS placement has to be designed in this section. Different from several existing DBS placement algorithms in drone-assisted mobile networks, which aim to maximize the network performance (such as network throughput or overall spectrum efficiency), we propose to jointly optimize DBS placement and bandwidth allocation in order to maximize the hovering time of the DBS and ensure the MUs' QoS in terms of the data rate requirements.

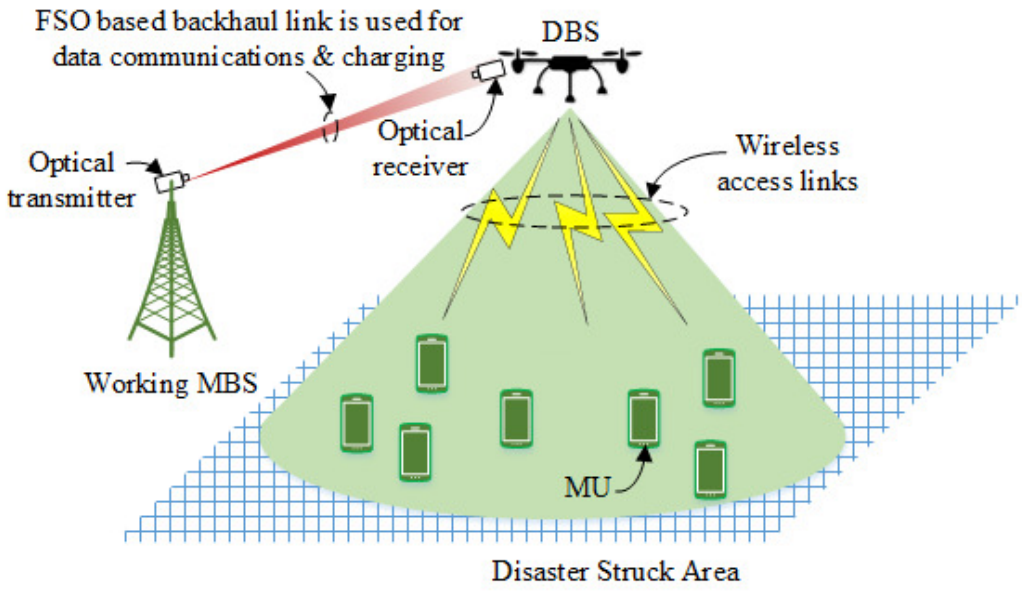


**Figure 4.10** FSO charging architecture.

### 4.2.1 FSO charging architecture

**Optical received power:** A working MBS transmits an optical beam carrying both data and energy to the DBS. The received optical power at the DBS ($P^r$) can be derived according to [5]. Here, the acquisition, pointing and tracking (APT) system [12] is assumed to be used in the architecture. Hence, the pointing error is not considered at the FSO receiver.

$$P^r = P^t \eta^t \eta^w, \tag{4.25}$$

where $P^t$ is the transmission power of the optical beam at the MBS, $\eta^t$ is the coefficient to convert electrical power into optical power, and $\eta^w$ is the environmental loss (caused by scattering and absorption of photons). Here, the environmental loss $\eta^w$ in Equation (4.25) can be estimated by [51]

$$\eta^w = 10^{-\frac{4.34\sigma d^{fso}}{10}}, \tag{4.26}$$

where $\sigma$ is the atmospheric attenuation coefficient, i.e., the amount of optical power loss in dB per kilometer. The distance between the DBS and its associated MBS ($d^{fso}$) is

$$d^{fso} = \sqrt{\left(\sum_{i \in \boldsymbol{I}} z_i \times \iota_i\right)^2 + (h - h^m)^2}, \tag{4.27}$$

where $h^m$ is the altitude of the associated MBS, $\iota_i$ is the horizontal distance between the associated MBS and location $i$, and $z_i$ is the location indicator, i.e., $z_i = 1$ when DBS $i$ is placed at location $i$; otherwise, $z_i = 0$. Thus, $\sum_{i \in \boldsymbol{I}} z_i \times \iota_i$ indicates the horizontal distance between the DBS and its associated MBS. Note that $\sigma$ in Equation (4.26) can be estimated by

$$\sigma = \frac{3.91}{v}\left(\frac{\lambda}{550}\right)^{-q}, \tag{4.28}$$

where $\lambda$ is the wavelength of the optical beam, $q$ is the size distribution of the scattering particles in the environment, and $v$ is the visibility range of the environment (i.e., the maximum distance that an object can be clearly discerned). The visibility range (in km) depends on the weather conditions and can be obtained from the field tests. For example, when the weather is clear, $v$ is normally larger than 50 km, but $v$ is less than 1 km in a foggy weather. Note that the value of $q$ is given by [51]

$$q = \begin{cases} 1.6, & v > 50, \\ 1.3, & 6 < v \leq 50, \\ 0.16v + 0.34, & 1 < v \leq 6, \\ v - 0.5, & 0.5 < v \leq 1, \\ 0, & v, \leq 0.5, \end{cases} \tag{4.29}$$

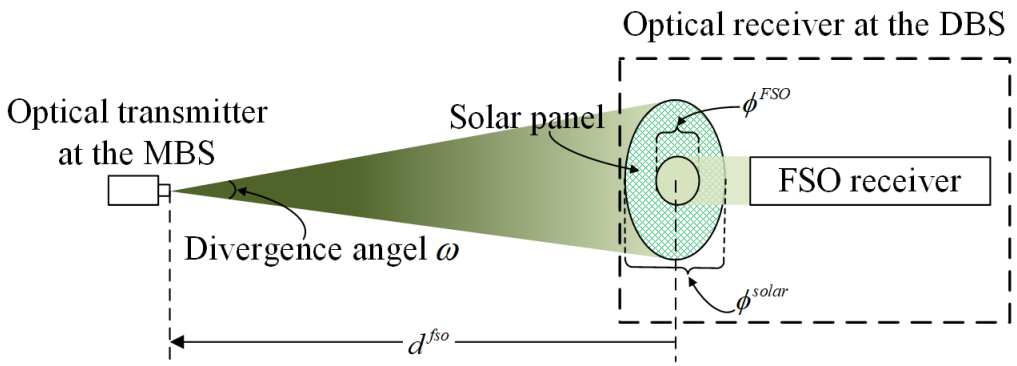


**Figure 4.11** Illustration of the received optical beam.

The optical beam received by the DBS is further separated into two portions. As illustrated in Figure 4.11, one portion is used by the solar panel, which converts the received optical power into electrical power to charge the battery of the DBS, and the other portion is used by the FSO receiver, which demodulates signals carried by the optical beam. Let $P^r$ be the total amount of power of the optical beam received by the DBS. Let $P^d$ and $P^c$ be the amount of optical power used for retrieving data

and charging the battery, respectively. Here,

$$P^r = P^d + P^c. \tag{4.30}$$

Note that, as shown in Figure 4.11, the size of the hole in the solar panel could change $P^c$ and $P^d$, i.e., a larger size of the hole indicates that a smaller portion of the received optical beam is received by the solar panel for charging the battery (i.e., smaller $P^c$) and a larger portion of the received optical beam is used to demodulate signals (i.e., larger $P^d$), and vice versa. Hence,

$$\begin{aligned} P^c &= (\tfrac{\phi^{FSO}}{\phi^{solar}})^2 P^r \\ P^d &= \left(1 - (\tfrac{\phi^{FSO}}{\phi^{solar}})^2\right) P^r, \end{aligned} \tag{4.31}$$

where $\phi^{FSO}$ and $\phi^{solar}$ ($\phi^{FSO} < \phi^{solar}$) are the diameters of the lens for the FSO receiver (i.e., the diameter of the hole) and the solar panel, respectively. Assume that the diameter of the optical beam at the solar panel (denoted as $d^{beam}$) is always equal to that of the solar panel no matter where the DBS is. This can be achieved by dynamically altering the divergence angle of the optical beam (denoted as $\omega$) based on the following equation,

$$\omega = 2 \arctan\left(\frac{\phi^{solar}/2}{d^{fso}}\right) = 2 \arctan\left(\frac{\phi^{solar}}{2d^{fso}}\right), \tag{4.32}$$

where $d^{fso}$ is calculated based on Equation (4.27).

**FSO-based backhaul data rate:** The achievable data rate of the FSO-based backhaul link from the associated MBS to the DBS is given by [5]

$$r^f = \frac{P^d}{E_p N_b}, \tag{4.33}$$

where $N_b$ is the sensitivity of the FSO receiver (at the DBS) in photons/bit, and $E_p$ is the amount of energy carried by a single photon, i.e., $E_p = h_p c/\lambda$ (here, $h_p$ is the Planck's constant, $c$ is the light speed, and $\lambda$ is the wavelength of the optical beam).

**Optical charging model:** Part of the received optical beam is used for charging batteries. Denote $\gamma$ as the charging efficiency to convert the received optical power $p^c$ into electrical power. The charging rate ($\hat{P}^c$) is

$$\hat{P}^c = \gamma P^c. \tag{4.34}$$

### 4.2.2 Joint bandwidth allocation DBS placement (TWIST) strategy

Assuming that a static number of MUs are located in a DSA, and different MUs have different data rate requirements. A DBS is placed over this DSA to provide services to these MUs. The energy consumption of the DBS comprises the communications and propulsion energy consumption. Normally, the propulsion system has higher energy demands than the communications system in a DBS, thus the propulsion energy consumption is approximately considered as the total power consumption of DBS (the power consumption of connumication is ignored). The propulsion energy consumption of a DBS can be further separated into two parts, i.e., the energy consumption of the DBS reaching the destination over the DSA and return to the control station (denoted as $E^{fly}$), and the DBS hovering energy consumption (denoted as $E^{hover}$). The value of $E^{fly}$ depends on $d^{fso}$, i.e.,

$$E^{fly} = \xi d^{fso}, \tag{4.35}$$

where $\xi$ indicates the average energy consumption of a drone by flying one km and $d^{fso}$ is the flying distance, which can be calculated based on Equation (4.27). The value of $E^{hover}$ depends on the hovering power consumption $P^{hover}$ and amount of hovering time $T$, i.e., $E^{hover} = P^{hover}T$. Denote $E^{battery}$ as the total amount of energy in the DBS's battery. Assuming that an optical link from the associated MBS to the DBS (to transmit data and energy) can be established once the DBS is stably hovering at the destination. Then, the maximum DBS hovering time with optical

charging is derived as follows.

$$T = \frac{E^{battery} - \xi d^{fso}}{P^{hover} - \hat{P}^c}. \tag{4.36}$$

The DBS's extra hovering time (denoted as $\Delta T$) is defined as the hovering time of the DBS with optical charging minus that without the optical charging, i.e.,

$$\Delta T = \frac{E^{battery} - \xi d^{fso}}{P^{hover} - \hat{P}^c} - \frac{E^{battery} - \xi d^{fso}}{P^{hover}}. \tag{4.37}$$

The problem of determining the DBS location as well as the amount of bandwidth in the access links is formulated as to maximize $\Delta T$, i.e.,

$$\textbf{P0:} \max_{z_i, h, b_j} \Delta T \tag{4.38}$$

$$s.t.: C1: \sum_{j \in \boldsymbol{J}} b_j \leq B, \tag{4.39}$$

$$C2: \sum_{i \in \boldsymbol{I}} h_i^{\min} z_i \leq h \leq h^{\max}, \tag{4.40}$$

$$C3: r_j \geq r_j^*, \tag{4.41}$$

$$C4: r^f \geq \sum_{j \in \boldsymbol{J}} r_j, \tag{4.42}$$

$$C5: \sum_{i \in \boldsymbol{I}} z_i = 1. \tag{4.43}$$

Here, C1 ensures that the bandwidth allocated to the MUs does not exceed the total amount of available bandwidth. C2 ensures the backhaul link is LoS (where $h_i^{min}$ is the minimum altitude to ensure the LoS between the DBS and its associated MBS when the DBS is deployed over location $i$, and $h^{max}$ is the maximum allowable altitude for the DBS). C3 indicates that each MU's data rate requirement should be guaranteed in the access link, where $r_j^*$ is the data rate requirement of MU $j$. C4 ensures the achievable backhaul link data rate to be no less than the achievable access link data rates. C5 implies that the DBS can only be deployed over one location.

The TWIST algorithm is proposed to solve **P0**. The intuition of TWIST is to first find a feasible DBS placement that can satisfy all the constraints in **P0**, and then look for a better DBS placement that reduces the distance to its associated MBS, thus increases $\Delta T$. TWIST is summarized in Algorithm 3.

**Initial 3-D DBS placement:** All the locations in the DSA are sorted in the ascending order based on $\iota_i$, i.e., the horizontal distance between location $i$ and its associated MBS. Let $\boldsymbol{I'}$ be the set of the ordered locations, i.e., $\boldsymbol{I'} = \{i \in \boldsymbol{I} \,|\iota_i \leq \iota_{i+1}\}$. Also, the initial altitude of the DBS is assumed to be $\max\{h^m, h_i^{min}\}$ (Assuming that $h_i^{max} \geq h^m, \forall i \in \boldsymbol{I}$), which incurs the shortest 3-D distance to the MBS among other possible altitudes. $h^m$ is the altitude of the MBS outside the DSA. The initial DBS placement is to iteratively deploy over location $i$ in $\boldsymbol{I'}$ with the altitude equal to $\max\{h^m, h_i^{min}\}$ until a feasible 3-D DBS placement, which can satisfy Constraints C1, C2, C3, and C4 in **P0**, has been found.

First, we select location $i$ in $\boldsymbol{I'}$ based on the ascending order of their horizontal distance. Then, we place the DBS over location $i$ with the altitude equal to $\max\{h^m, h_i^{min}\}$. For each MU, the pathloss from the DBS to the MU (i.e., $\bar{\eta}_j$) is calculated based on Equation (3.9). Afterward, we calculate the amount of bandwidth that satisfies its the minimum data rate requirement in C3, i.e.,

$$b_j = r_j^* / \log\left(1 + \frac{p \cdot 10^{-\bar{\eta}_j/10}}{N_0}\right). \tag{4.44}$$

The achievable data rate of the FSO-based backhaul link (i.e., $r_i^f$) is calculated based on Equation (4.12). If $\sum_{j \in \boldsymbol{J}} b_j \leq B$ (i.e., C1) and $r_i^f \geq \sum_{j \in \boldsymbol{J}} r_j^*$ (i.e., C4) can be satisfied, then location $i$ and its altitude $\max\{h^m, h_i^{min}\}$ are the initial optimal 3-D placement for the DBS, i.e., $i^* = i$ (i.e., $z_{i^*} = 1$) and $h^* = \max\{h^m, h_{i^*}^{min}\}$; otherwise, the next location in $\boldsymbol{I'}$ will be selected to check if it is a feasible DBS placement by executing Steps 1-5 in Algorithm 3.

Let $d_{i^*}^{fso}$ be the 3-D distance between the DBS and its associated MBS if the DBS is deployed in its initial 3-D placement (i.e., $\langle x_{i^*}, y_{i^*}, \max\{h^m, h_{i^*}^{min}\}\rangle$, where $x_{i^*}$ and $y_{i^*}$ indicate the latitude and longitude of location $i^*$, respectively). Based on Equation (4.27), then

$$d_{i^*}^{fso} = \sqrt{(\iota_{i^*})^2 + (\max\{h^m, h_{i^*}^{min}\} - h^m)^2}, \tag{4.45}$$

where $\iota_{i^*}$ is the horizontal distance between the associated MBS and location $i^*$.

**Recursive search:** Based on Equation (4.37), it is easy to derive that reducing $d^{fso}$ could increase the extra hovering time of the DBS ($\Delta T$). Recursive searching is to backtrack the locations whose indices are lower than $i^*$ in $\boldsymbol{I}'$ in order to find a better 3-D placement for the DBS that could reduce $d^{fso}$ while satisfying all the constraints in **P0**. That is, the DBS will be iteratively deployed over one of these locations and the DBS adjust its altitude to find a better 3-D placement. Let $k = i^*$ and we iteratively select a location in $\boldsymbol{I}'$ according to the order of $\langle k-1, k-2, \cdots, 1\rangle$. Denote $i$ as the selected location in the current iteration. Deploying the DBS over location $i$ could be a better 3-D placement if $d_i^{fso}$ is reduced, i.e., $\sqrt{{\iota_i}^2 + (h_i - h^m)^2} < d_{i^*}^{fso}$, where $d_{i^*}^{fso}$ is derived from Equation (4.45). Thus, $h_i \leq \sqrt{\left(d_{i^*}^{fso}\right)^2 - {\iota_i}^2} + h^m$ is acquired. The next step (i.e., Step 3)) is to find all the possible values of $h_i$ to satisfy all the constraints in **P0**, where $h_i^{\min} \leq h_i \leq \min\left\{\sqrt{\left(d_{i^*}^{fso}\right)^2 - {\iota_i}^2} + h^m, h^{\max}\right\}$. Note that if $h_i^{\min} > \sqrt{\left(d_{i^*}^{fso}\right)^2 - {\iota_i}^2} + h^m$, then deploying the DBS over location $i$ cannot be a better 3-D placement.

Denote $\Delta h$ as the step size of adjusting the altitude and we iteratively select the value of $h_i$ from the order $\left\{h_i^{\min}, h_i^{\min} + \Delta h, h_i^{\min} + 2\Delta h, \cdots\right\}$ until $h_i > \min\left\{\sqrt{\left(d_{i^*}^{fso}\right)^2 - {\iota_i}^2}, h^{\max}\right\}$ In each iteration, we check whether the selected $h_i$ is a feasible solution to meet all the constraints or not. If $h_i$ is a feasible solution, we put it into set $\boldsymbol{H}_i$. After finishing all the iterations, if $\boldsymbol{H}_i = \emptyset$, then deploying the

DBS over location $i$ is not a better DBS placement; otherwise, find the altitude $\bar{h}_i$ that incurs the shortest distance to the associated MBS among other altitudes in $\boldsymbol{H}_i$, i.e., $\bar{h}_i = \arg\min_{h_i \in \boldsymbol{H}_i} |h_i - h^m|$. We next calculate $d_i^{fso}$ based on Equation (4.45), where $d_i^{fso}$ is the 3-D distance between the DBS and its associated MBS when the DBS is placed over location $i$ with the altitude equal to $\bar{h}_i$. If $d_i^{fso} < d_{i^*}^{fso}$, the optimal DBS placement becomes $i^* = i$ (i.e., $z_{i^*} = 1$) and $h^* = \bar{h}_i$. We iteratively select the next location in $\boldsymbol{I}'$ by executing Steps 1-3 in Algorithm 3 to update the the optimal DBS placement $\langle i^*, h^* \rangle$ until all the locations have been selected.

**Algorithm 3** TWIST

Initialize $\boldsymbol{I}'$.
**for** $i = 1,\ i \leq |\boldsymbol{I}'|,\ i = i + 1$ **do**
  Set $x_i = 1$;
  $h = \max\{h^m, h_i^{min}\}$;
  $\forall j \in \boldsymbol{J}$, calculate $\bar{\eta}_j$ based on Equation (3.9);
  $\forall j \in \boldsymbol{J}$, calculate $b_j$ based on Equation (4.44);
  Calculate $r_i^f$ based on Equation (4.12);
  **if** $\sum_{j \in \boldsymbol{J}} b_j \leq B$ and $r_i^f \geq \sum_{j \in \boldsymbol{J}} r_j^*$ **then**
    $i^* = i$, $z_{i^*} = 1$, and $h^* = \max\{h^m, h_{i^*}^{min}\}$;
  **else**
    $z_i = 0$;
  **end if**
**end for**
Calculate $d_{i^*}^{fso}$ based on Equation (4.45).
$k = i^*$.
**for** $i = k - 1,\ i \geq 1,\ i = i - 1$ **do**
  $x_i = 1$;
  **for** $h_i = h_i^{min}, h_i \leq \min\left\{\sqrt{\left(d_{i^*}^{fso}\right)^2 - \iota_i{}^2}, h^{\max}\right\},\ h = h + \Delta h$ **do**

$\forall j \in \boldsymbol{J}$, calculate $\bar{\eta}_j$ based on Equation (3.9)

$\forall j \in \boldsymbol{J}$, calculate $b_j$ based on Equation (4.44)

Calculate $r_i^f$ based on Equation (4.12);

**if** $\sum_{j \in \boldsymbol{J}} b_j \leq B$ and $r_i^f \geq \sum_{j \in \boldsymbol{J}} r_j^*$ **then**

  $\boldsymbol{H}_i = \boldsymbol{H}_i \cap h_i$;

**end if**

**end for**

**if** $\boldsymbol{H}_i = \emptyset$ **then**

  $z_i = 0$;

**else**

  $\bar{h}_i = \arg\min_{h_i \in \boldsymbol{H}_i} |h_i - h^m|$;

  Calculate $d_i^{fso} = \sqrt{(\iota_i)^2 + (\bar{h}_i - h^m)^2}$;

  **if** $d_i^{fso} < d_{i^*}^{fso}$ **then**

    $z_{i^*} = 0$, $i^* = i$, $z_{i^*} = 1$, and $h^* = \bar{h}_i$;

  **else**

    $z_i = 0$;

  **end if**

**end if**

**end for**

### 4.2.3 Simulation results

The performance of TWIST is evaluated via simulations by comparing TWIST with two other baseline algorithms, i.e., CLP (center location placement) [10] and MTP (maximal throughput placement) [16]. In CLP, the DBS is first deployed at the center of all the MUs, and then the altitude of the DBS and the bandwidth assignment are adjusted to satisfy the data rate requirements of all the MUs in the access links. The intuition of MTP is to derive the optimal DBS placement such that the total

**Table 4.3** Simulation Parameters III

| | |
|---|---|
| FSO transmission power [63] | 100 Watt |
| Divergence angle ($\theta_g$) | 1 $mrad$ |
| Noise power spectral density ($N_0$) | -104 $dBm/Hz$ |
| Receiver radius ($r$) | 0.05 $m$ |
| Receiver sensitivity ($N_b$) [28] | $2 \times 10^5 photons/bit$ |
| FSO wavelength ($\lambda$) | 1550 $nm$ |
| Environment index ($\beta$) [49] | 0.16 |
| Environment index ($b$) [49] | 9.61 |
| FSO charging efficiency ($\gamma$) | 20% |
| Maximum altitude of DBS ($f^{max}$) | 300 $m$ |
| The altitude of working MBS ($h^m$) | 20 $m$ |
| DBS power consumption ($P^{hover}$) | 100 Watt |
| DBS battery capacity ($E^{battery}$) | 65 Wh |
| Carrier frequency ($f_c$) | 2 $GHz$ |
| DBS transmission power ($p$) | 40 $dBm$ |

achievable data rates of the MUs in downloading data from the associated MBS via the DBS is maximized. Both TWIST and MTP assume that FSO is applied in the backhaul communications.

Assume that a DSA forms a rectangle area with the range of $\langle 0 \sim 1 \text{ km}, 0 \sim 1 \text{ km} \rangle$. The DSA is further divided into 40,000 locations, and size of each location is 50 m $\times$ 50 m. The working MBS is placed at $\langle -100 \text{ m}, -100 \text{ m} \rangle$. Initially, there are 40 MUs uniformly distributed in the DSA. The data rate requirements of these MUs follow a normal distribution with the mean and standard deviation equal to 2 Mbps and 1 Mbps, respectively. The rest of the simulation parameters are listed in Table 4.3.

The extra hovering time for the three algorithms when the amount of available bandwidth in the access links is varying from 20 MHz to 17.5 MHz is shown in Figure. 4.12. The visibility range is $v = 0.9$ km. The figure shows that TWIST always achieves the longest extra hovering time as compared to MTP and CLP. Also, the extra hovering time incurred by the three algorithms increases as the amount of available bandwidth in the access links decreases. This is because as the amount of available bandwidth decreases, each MU can be allocated with less bandwidth in the access link, thus the DBS needs to be placed over a location that incurs better channel gain to the MUs in order to satisfy their data rate requirements. The location incurring better channel gain to the MUs in the access links normally leads to a longer distance in the backhaul link, and $\Delta T$ is reduced accordingly. For example, Figure 4.13 exhibits the placements of the DBS acquired by the three algorithms. Here, the locations with orange and blue color imply the DBS locations (incurred by the three algorithms) when the amount of available bandwidth are 18 MHz and 20 MHz, respectively. In the figure, as the available bandwidth changes from 20 MHz to 18 MHz, the location of the DBS incurred by the three algorithms moves farther away from its associated MBS; this reduces the charging rate $\hat{P}^c$, and decreases the extra hovering time. Note that, as shown in Figure 4.12, the difference of the extra hovering time between TWIST and MTP/CLP increases as the amount of available bandwidth in the access links decreases.

How the visibility range $v$ affects $\Delta T$ is shown in Figure 4.14. As mentioned before, the visibility range $v$ is normally determined by the weather conditions in the area. The available bandwidth in the access links is 20 MHz. A larger $v$ results in a higher charging rate and a lower pathloss leads to a larger backhaul capacity. The figure shows that the extra hovering time for the three algorithms decreases when $v$ decreases because the charging rate decreases as $v$ decreases. Meanwhile, the difference of the extra hovering time between TWIST and MTP/CLP also reduces

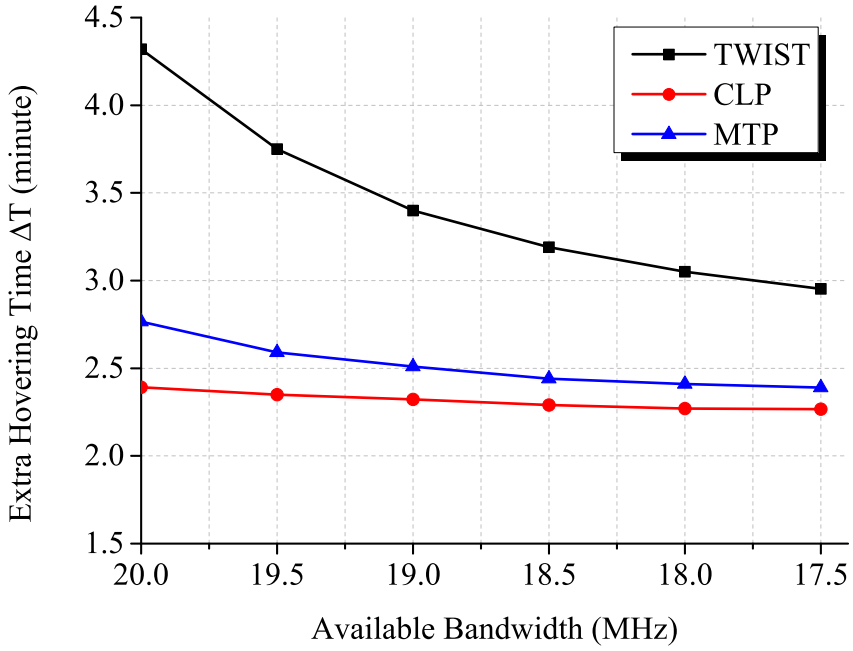


**Figure 4.12** Extra hovering time by varying available bandwidth.

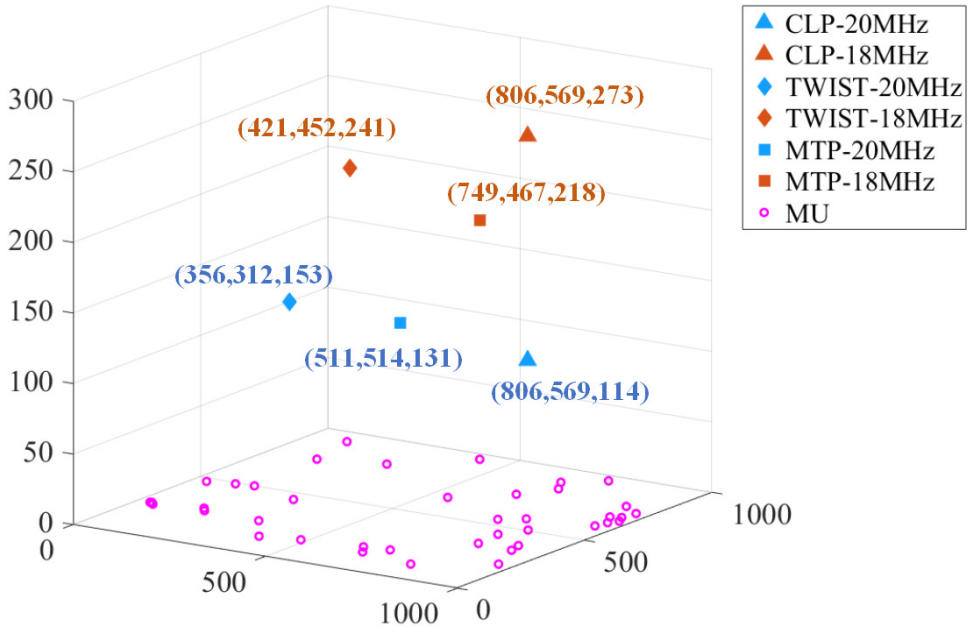


**Figure 4.13** DBSs locations with different available bandwidth.

as $v$ decreases. Although the DBS placement incurred by TWIST leads to a shorter backhaul link than those incurred by CLP and MTP, the amount of charging rate gain (which is caused by a shorter backhaul link) decreases as $v$ decreases.

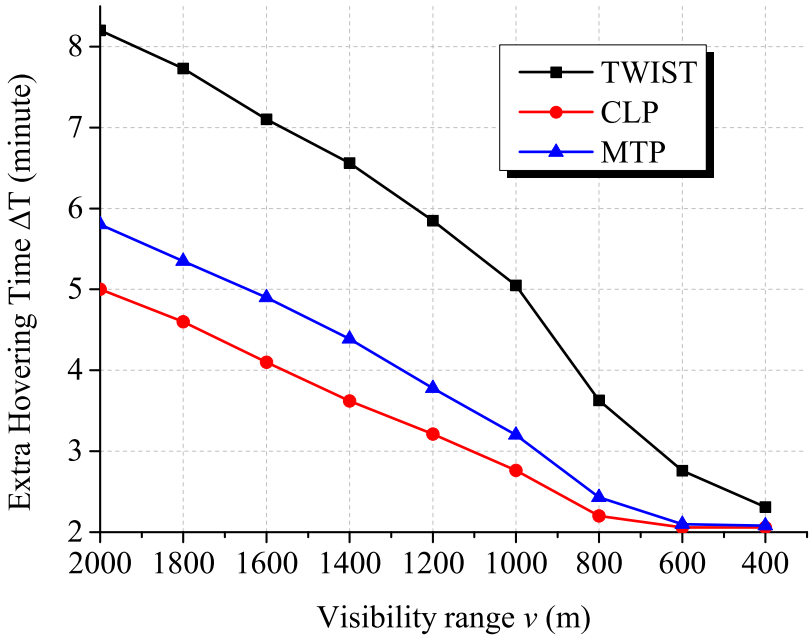


**Figure 4.14** Extra hovering time by varying visibility range.

# CHAPTER 5

# FUTURE WORK

Drone-assisted network has been proposed in Chapter 2 to help provision service in disaster-struck areas. The primary objective of a rescue mission is to quickly locate victims in the disaster struck area [32], i.e., the victim detection. Current victim detection can be carried out by three different methods. The first method is to deploy radar to detect victims. Radar has been widely used to detect objects in long distance by changing the wavelength and the signal energy [9]. For example, the infrared ray radar can easily detect the alive victims. Since the infrared ray has very low penetrability, the infrared ray radar cannot find the victims buried in the ruins or covered by shelters [33].

The second method to detect victims through live videos. Machine learning algorithms have been adopted to analyze live videos in real time. By transmitting the live stream videos from the DBS to its associated MBS, the MBS can analyze the videos to find the victims in the videos. Given the location of the DBS, the associated MBS can perform further analysis to estimate the location of the detected victim. However, current victim detection algorithms with live streams are only capable of detecting victims close to the camera, e.g., less than 10 meters [27]. In this case, the live video victim detection is suitable for perticular recusing drones, i.e., drones flying at low altitude to search for victims. Considering the large computing resource requirements for the live stream victim detection (e.g., using convolutional neural network (CNN) [53] to detect victims), a DBS has to transmit the live stream to its associated MBS for analysis. A large backhaul capacity between a DBS and its associated MBS is necessary to enable live stream victim detection.

The third method is to detect victims through photos. Unlike detecting victims through live stream videos, detecting victims from photos is not sensitive to delay. To detect victims in photos, the manager only needs to decide whether there exists a victim in a photo or not, rather than to figure out where the victim is [19]. Thus, victim detection can be simplified as a logic regression problem. In this case, the machine learning algorithms for logic regression can be used to detect victims. For example, support vector machine (SVM) is a low complexity algorithm to facilitate logic regression [41] and it can be tailored for victim detection. By using SVM, the DBS can detect victim by itself, rather than transmitting all the captured data (i.e., the photos) to its associated MBS. In this case, the backhaul is not the transmission bottleneck and the DBS can be placed more flexibly.

In order to increase the accuracy of machine learning, generating a suitable training data set is necessary. However, the groud situation of disaster struck areas varies with different disaster types and the location of the disaster. Generating a training data set for each disaster is hard but important to increase the detection accuracy. Currently, most researches about machine learning focus on the training algorithms. The dataset for training and testing are always pre-defined. We plan to propose a drone-assisted system to facilitate victim detection, which can generate the training data set for machine learning and can train the model simultaneously, as shown in Figure 5.1.

Considering the limited backhaul bandwidth, the federated learning is used to train the model of victim detection. In this case, the training and testing for victim detection can be done by the drone and the MUs. In this case, the drone does not need to transmit the huge amount of labeled data to its associated MBS.

The mechanism of the federated learning is illustrated in Figure 5.2. The drone will download a raw model from its associated MBS prior to activating federated

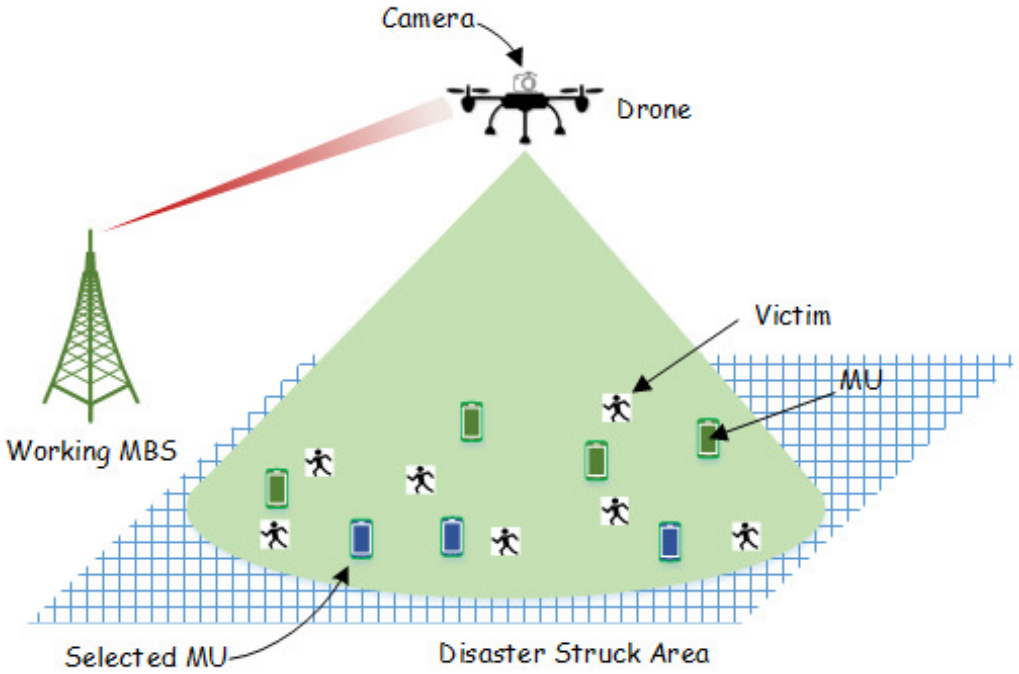


**Figure 5.1** Drone based victim detection architecture.

learning. A raw model is a pre-trained machine learning model, which can perform victim detection with low accuracy [61]. The mechanism mainly consists of five steps:

Step 1. Preparing: A drone carries a pre-trained model hovering above the disaster-struck area at a suitable location. The drone establishes communication links with MUs. The drone will select MUs based on some algorithm from served MUs. Based on the computing capacity of selected MUs, the drone will calculate the "global training timeslot" and the training dataset requirements (i.e., how many photos per training per MU). After that, the drone will send the pre-trained model to these MUs.

Step 2. Dataset generating: After the MUs have received the model, these MUs will take several pictures of their surroundings. The MUs will label the photos with "having victims" or "no victims". After the MUs take enough number of photos, they will start training the data.

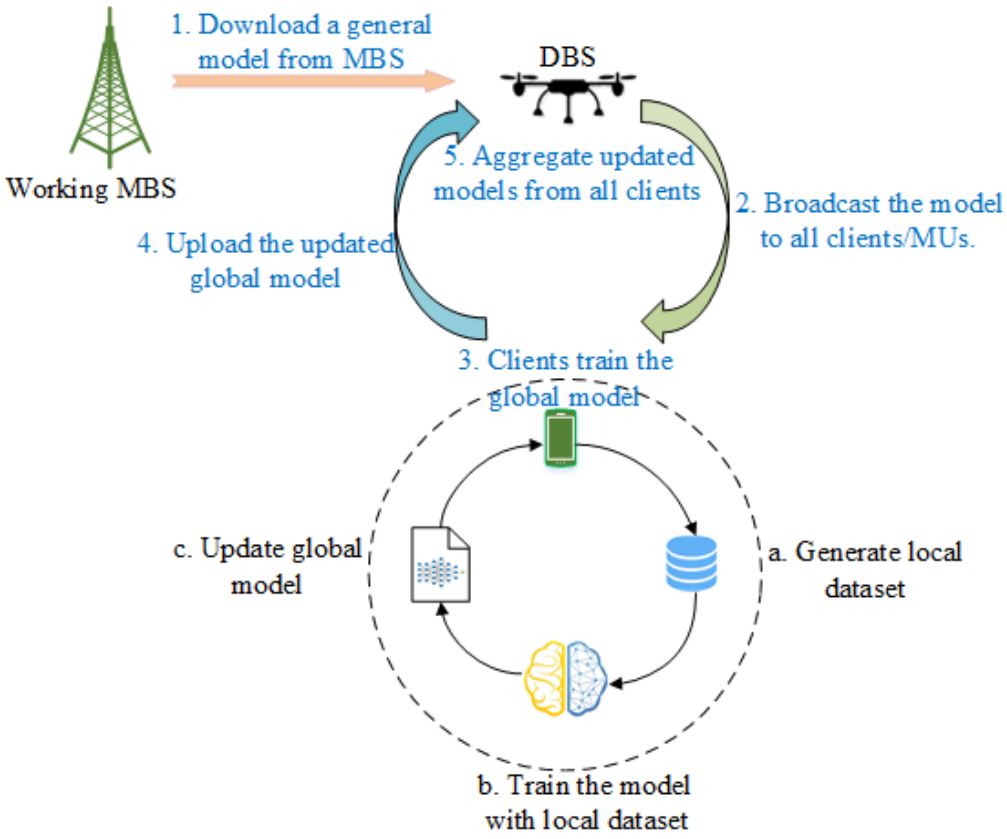


**Figure 5.2** Mechanism of federated learning based victim detection in drone-assisted network.

Step 3. Model training: Based on the photos taken by each MU, they will use these labeled photos for a surprised learning. Once a MU has finished training the data, it will send the updated model back to the DBS.

Step 4. Model aggregation: The drone will start aggregating the models after it has received all models from the selected MUs. By using an aggregation strategy, the drone will generate a new model and send it back to the MUs.

Step 5. Accuracy check: The selected MUs will repeat Step 2 with the new model and test the accuracy of this new model. If the accuracy of this model is higher than the required accuracy, then this MU will return its results to the drone and stop training this model. If the accuracy is not satisfied, this MU will continue the model training (i.e., Step 3).

Although the proposed architecture can solve the problem of victim detection, there remain many challenges such as participant selection [13]. In federated learning, the drone can start a new iteration only after it has received all updated models from MUs. Thus, choosing participating MUs (the MUs that are chosen to help federated learning are called participating MUs) can greatly influence the minimum timeslot of each iteration. Our future work will focus on designing a suitable client selection strategy to accelerate the training time for victim detection.

# CHAPTER 6

# CONCLUSION

DBSs have been proposed to extend coverage and improve communications between MUs and their corresponding MBSs. Different from the base stations on the ground, DBSs can flexibly fly over and close to MUs to establish a better vantage for communications. Thus, the pathloss between a DBS and an MU can be much smaller than that between the MU and MBS. In addition, by hovering in the air, the DBS can likely establish a LoS link to the MBS. DBSs can be leveraged to recover communications in a large natural disaster struck area and to fully embody the advantage of drone-assisted communications. In order to retrieve signals from MUs in a large disaster struck area, DBSs need to overcome the large pathloss incurred by the long distance between DBSs and MBSs. This has been addressed by the following two strategies.

First, placing multiple drones in a disaster struck area can be used to mitigate the problem of a large backhaul pathloss. In this method, data from MUs in the disaster struck area may be forwarded by more than one drone, i.e., DBSs can enable drone-to-drone communications. The throughput from the disaster struck area can potentially be enhanced by this multi-drone strategy. A cooperative DBS placement and channel allocation algorithm has been proposed to maximize the aggregated data rate from MUs in a disaster struck area. It has been demonstrated by simulations that the aggregated data rate can be improved by more than 10%, as compared to the scenario without drone-to-drone communications.

Second, FSO has been used as the backhaul links to reduce the backhaul pathloss. FSO can provision a high-speed point-to-point transmission and is suitable for the backhaul transmission. A heuristic algorithm has been proposed to maximize

the number of MUs that can be served by the drones by optimizing user association, DBS placement and spectrum allocation iteratively. It has been demonstrated by simulations that the proposed algorithm can cover over 15% more MUs at the expense of less than 5% of the aggregated throughput. Equipping DBSs and MBSs with FSO transceivers incurs extra payload for DBSs, hence shortening the hovering time of DBSs. To prolong the hovering time of a DBS, the FSO beam is deployed to facilitate simultaneous communications and charging. The viability of this concept has been studied by varying the distance between a DBS and an MBS, in which an optimal location of the DBS is found to maximize the data throughput, while the charging power directed to the DBS from the MBS diminishes with the increasing distance between them.

The future work has been planned to incorporate artificial intelligence to enhance drone-assisted networking for various applications. For example, a drone equipped with a camera can be used to detect victims. By analyzing the captured pictures, the locations of the victims can be estimated by some machine learning based image processing technology.

# BIBLIOGRAPHY


[1] S. Ahmed, M. Z. Chowdhury, and Y. M. Jang. Energy-efficient UAV-to-user scheduling to maximize throughput in wireless networks. *IEEE Access*, 8:21215–21225, 2020.

[2] H. Ajam, M. Najafi, V. Jamali, and R. Schober. Ergodic sum rate analysis of UAV-based relay networks with mixed RF-FSO channels. *IEEE Open Journal of the Communications Society*, 1:164–178, 2020.

[3] A. Al-Hourani, S. Kandeepan, and S. Lardner. Optimal LAP altitude for maximum coverage. *IEEE Wireless Communications Letters*, 3(6):569–572, Dec. 2014.

[4] A. Alsharoa, H. Ghazzai, A. Kadri, and A. E. Kamal. Energy management in cellular HetNets assisted by solar powered drone small cells. In *IEEE Wireless Communications and Networking Conference (WCNC)*, pages 1–6, Mar. San Francisco, CA, 2017.

[5] M. Alzenad, M. Z. Shakir, H. Yanikomeroglu, and M. Alouini. FSO-Based vertical backhaul/fronthaul framework for 5G+ wireless networks. *IEEE Communications Magazine*, 56(1):218–224, Jan. 2018.

[6] R. Amorim, P. Mogensen, T. Sorensen, I. Z. Kovacs, and J. Wigard. Pathloss measurements and modeling for UAVs connected to cellular networks. In *IEEE 85th Vehicular Technology Conference (VTC Spring)*, pages 1–6, Sydney, 2017.

[7] N. Ansari, Q. Fan, X. Sun, and L. Zhang. Soarnet. *IEEE Wireless Communications*, 26(6):37–43, Dec. 2019.

[8] N. Ansari, D. Wu, and X. Sun. FSO as backhaul and energizer for drone-assisted mobile access networks. *ICT Express*, 2020.

[9] T. Anugraha, K. Anwar, and S. P. W. Jarot. Cellular communications-based detection to estimate location of victims post-disaster. In *Symposium on Future Telecommunication Technologies (SOFTT)*, volume 1, pages 1–5, Kuala Lumpur, 2019.

[10] N. N. Bhuiyan, R. T. Ratri, I. Anjum, and M. A. Razzaque. Traffic-load aware spectrum allocation in cloud assisted cognitive radio networks. In *IEEE Region 10 Humanitarian Technology Conference (R10-HTC)*, pages 598–601, Dec. Dhaka, 2017.

[11] R. I. Bor-Yaliniz, A. El-Keyi, and H. Yanikomeroglu. Efficient 3-D placement of an aerial base station in next generation cellular networks. In *IEEE International Conference on Communications (ICC)*, pages 1–5, May. Kuala Lumpur, 2016.

[12] M. Borrello. A multi stage pointing acquisition and tracking (PAT) control system approach for air to air laser communications. In *American Control Conference.*, pages 3975–3980, Jun. Portland, OR, 2005.

[13] B. Brik, A. Ksentini, and M. Bouaziz. Federated learning for UAVs-enabled wireless networks: Use cases, challenges, and open problems. *IEEE Access*, 8:53841–53849, 2020.

[14] A. Chaaban, J. Morvan, and M. Alouini. Free-space optical communications: Capacity bounds, approximations, and a new sphere-packing perspective. *IEEE Transactions on Communications*, 64(3):1176–1191, Mar. 2016.

[15] J. Chen, L. Yang, W. Wang, H. Yang, Y. Liu, M. O. Hasna, and M. Alouini. A novel energy harvesting scheme for mixed FSO-RF relaying systems. *IEEE Transactions on Vehicular Technology*, 68(8):8259–8263, Aug. 2019.

[16] J. Cho and J. Kim. Performance comparison of heuristic algorithms for UAV deployment with low power consumption. In *International Conference on Information and Communication Technology Convergence (ICTC)*, pages 1067–1069, Oct. Jeju, 2018.

[17] Y. Choi and H. Shirani-Mehr. Simultaneous transmission and reception: Algorithm, design and system level performance. *IEEE Transactions on Wireless Communications*, 12(12):5992–6010, Dec. 2013.

[18] N. Cvijetic, D. Qian, J. Yu, Y. Huang, and T. Wang. 100 Gb/s per-channel free-space optical transmission with coherent detection and MIMO processing. In *35th European Conference on Optical Communication*, pages 1–2, Sep. Vienna, 2009.

[19] N. Dalal and B. Triggs. Histograms of oriented gradients for human detection. In *IEEE Computer Society Conference on Computer Vision and Pattern Recognition (CVPR'05)*, volume 1, pages 886–893, San Diego, CA, 2005.

[20] H. Falaki, D. Lymberopoulos, R. Mahajan, S. Kandula, and D. Estrin. A first look at traffic on smartphones. In *10th ACM SIGCOMM conference on Internet measurement*, pages 281–287. ACM, New York, NY, 2010.

[21] W. Fawaz, C. Abou-Rjeily, and C. Assi. UAV-aided cooperation for FSO communication systems. *IEEE Communications Magazine*, 56(1):70–75, Jan. 2018.

[22] A. Fotouhi, M. Ding, and M. Hassan. Flying drone base stations for macro hotspots. *IEEE Access*, 6:19530–19539, 2018.

[23] B. Galkin, J. Kibilda, and L. A. DaSilva. Backhaul for low-altitude UAVs in urban environments. In *IEEE International Conference on Communications (ICC)*, pages 1–6, May. Kansas City, MO, 2018.

[24] Z. Gu, J. Zhang, Y. Ji, L. Bai, and X. Sun. Network topology reconfiguration for FSO-based fronthaul/backhaul in 5G+ wireless networks. *IEEE Access*, 6:69426–69437, 2018.

[25] Y. Guo, S. Yin, and J. Hao. Joint placement and resources optimization for multi-user UAV-relaying systems with underlaid cellular networks. *IEEE Transactions on Vehicular Technology*, pages 1–1, 2020.

[26] L. Gupta, R. Jain, and G. Vaszkun. Survey of important issues in UAV communication networks. *IEEE Communications Surveys Tutorials*, 18(2):1123–1152, 2016.

[27] D. R. Hartawan, T. W. Purboyo, and C. Setianingsih. Disaster victims detection system using convolutional neural network (CNN) method. In *IEEE International Conference on Industry 4.0, Artificial Intelligence, and Communications Technology (IAICT)*, pages 105–111, BALI, 2019.

[28] G. Hu, C. Chen, and Z. Chen. Free-space optical communication using visible light. *Journal of Zhejiang University-SCIENCE A*, 8(2):186–191, 2007.

[29] L. Ji, J. Chen, and Z. Feng. Spectrum allocation and performance analysis for backhauling of UAV assisted cellular network. *China Communications*, 16(8):83–92, 2019.

[30] R. Jin, L. Yang, and H. Zhang. Performance analysis of temporal correlation in finite-area UAV networks with LoS/NLoS. In *IEEE Wireless Communications and Networking Conference (WCNC)*, pages 1–6, Seoul, 2020.

[31] E. Kalantari, H. Yanikomeroglu, and A. Yongacoglu. On the number and 3D placement of drone base stations in wireless cellular networks. In *IEEE Vehicular Technology Conference. (VTC-Fall)*, pages 1–6, Sep. Montreal, QC, 2016.

[32] A. M. Koushik, F. Hu, and S. Kumar. Deep $Q$ -learning-based node positioning for throughput-optimal communications in dynamic UAV swarm network. *IEEE Transactions on Cognitive Communications and Networking*, 5(3):554–566, 2019.

[33] C. Labarthe, J. Mutzig, B. Jecko, H. Hamieh, E. Martinod, N. Feix, J. M. Lalande, J. Denoual, J. Floch, V. Bertrand, R. Vergnault, P. Minvielle, and F. Ducasse. An ultra-wideband radar concept for the detection of buried victims beneath building rubble. In *International Radar Conference "Surveillance for a Safer World" (RADAR)*, pages 1–6, Bordeaux, 2009.

[34] J. H. Lee, K. H. Park, Y. C. Ko, and M. S. Alouini. Throughput maximization of mixed FSO/RF UAV-aided mobile relaying with a buffer. *IEEE Transactions on Wireless Communications*, pages 1–1, 2020.

[35] C. Liu, C. Jiang, and C. Qiu. Overview of coil designs for wireless charging of electric vehicle. In *IEEE PELS Workshop on Emerging Technologies: Wireless Power Transfer (WoW)*, pages 1–6, May. Chongqing, 2017.

[36] S. Liu, Z. Wei, Z. Guo, X. Yuan, and Z. Feng. Performance analysis of UAVs assisted data collection in wireless sensor network. In *IEEE 87th Vehicular Technology Conference (VTC Spring)*, pages 1–5, Jun. Porto, 2018.

[37] Y. Liu, K. Liu, J. Han, L. Zhu, Z. Xiao, and X. G. Xia. Resource allocation and 3D placement for UAV-enabled energy-efficient IoT communications. *IEEE Internet of Things Journal*, pages 1–1, 2020.

[38] Y. Lu, W. Wang, and B. Bhargava. Hierarchical structure for supporting movable base stations in wireless networks. In *10th International Conference on Telecommunications.*, volume 1, pages 729–736, Feb. Papeete, 2003.

[39] K. Mase. Communication service continuity under a large-scale disaster: Providing a wireless multihop network and shelter communication service for a disaster area under the great east japan earthquake. In *IEEE International Conference on Communications (ICC)*, pages 6314–6318, Jun. Ottawa, ON, 2012.

[40] M. Najafi, H. Ajam, V. Jamali, P. D. Diamantoulakis, G. K. Karagiannidis, and R. Schober. Statistical modeling of the FSO fronthaul channel for UAV-based communications. *IEEE Transactions on Communications*, 68(6):3720–3736, 2020.

[41] S. Nakajima, T. Yamasaki, K. Matsumoto, K. Uemura, T. Wada, and K. Ohtsuki. Behavior recognition and disaster detection by the abnormal analysis using SVM for ERESS. In *International Conference on Information Networking (ICOIN)*, pages 646–651, Chiang Mai, 2018.

[42] M. Narang, W. Liu, J. Gutierrez, and L. Chiaraviglio. A cyber physical buses-and-drones mobile edge infrastructure for large scale disaster emergency communications. In *IEEE 37th International Conference on Distributed Computing Systems Workshops (ICDCSW)*, pages 53–60, Jun. Atlanta, GA, 2017.

[43] R. Rajashekar, M. D. Renzo, K. V. S. Hari, and L. Hanzo. A generalized transmit and receive diversity condition for feedback-assisted MIMO systems: Theory and applications in full-duplex spatial modulation. *IEEE Trans. Signal Process.*, 65(24):6505–6519, Dec. 2017.

[44] P. Rawat, M. Haddad, and E. Altman. Towards efficient disaster management: 5G and device to device communication. In *International Conference on Information and Communication Technologies for Disaster Management (ICT-DM)*, pages 79–87, Nov. Rennes, 2015.

[45] L. Ruan, J. Wang, J. Chen, Y. Xu, Y. Yang, H. Jiang, Y. Zhang, and Y. Xu. Energy-efficient multi-UAV coverage deployment in UAV networks: A game-theoretic framework. *China Communications*, 15(10):194–209, 2018.

[46] L. Ruan, J. Wang, J. Chen, Y. Xu, Y. Yang, H. Jiang, Y. Zhang, and Y. Xu. Energy-efficient multi-UAV coverage deployment in UAV networks: A game-theoretic framework. *China Communications*, 15(10):194–209, 2018.

[47] T. Sakano, S. Kotabe, T. Komukai, T. Kumagai, Y. Shimizu, A. Takahara, T. Ngo, Z. M. Fadlullah, H. Nishiyama, and N. Kato. Bringing movable and deployable networks to disaster areas: development and field test of MDRU. *IEEE Network*, 30(1):86–91, Jan. 2016.

[48] K. Sang-Won, C. In-Kui, and H. Sung-Yong. Comparison of charging region differences according to receiver structure in drone wireless charging system. In *International Conference on Information and Communication Technology Convergence (ICTC)*, pages 1058–1060, Oct. Jeju, 2017.

[49] W. Shi, J. Li, W. Xu, H. Zhou, N. Zhang, S. Zhang, and X. Shen. Multiple drone-cell deployment analyses and optimization in drone assisted radio access networks. *IEEE Access*, 6:12518–12529, 2018.

[50] M. Shin, J. Kim, and M. Levorato. Auction-based charging scheduling with deep learning framework for multi-drone networks. *IEEE Transactions on Vehicular Technology*, 68(5):4235–4248, May. 2019.

[51] S. Singh and G. Soni. Pointing error evaluation in FSO link. In *Fifth International Conference on Advances in Recent Technologies in Communication and Computing (ARTCom)*, pages 365–370, Sep. Bangalore, 2013.

[52] C. Singhal and K. Rahul. Efficient QoS provisioning using SDN for end-to-end data delivery in UAV assisted network. In *IEEE International Conference on Advanced Networks and Telecommunications Systems (ANTS)*, pages 1–6, GOA, 2019.

[53] I. A. Sulistijono and A. Risnumawan. From concrete to abstract: Multilayer neural networks for disaster victims detection. In *International Electronics Symposium (IES)*, pages 93–98, Denpasar, 2016.

[54] X. Sun and N. Ansari. EdgeIoT: Mobile edge computing for the internet of things. *IEEE Communications Magazine*, 54(12):22–29, Dec. 2016.

[55] X. Sun and N. Ansari. Latency aware drone base station placement in heterogeneous networks. In *IEEE Global Communications Conference*, pages 1–6, Dec. Singapore, 2017.

[56] X. Sun, N. Ansari, and R. Fierro. Jointly optimized 3D drone mounted base station deployment and user association in drone assisted mobile access networks. *IEEE Transactions on Vehicular Technology*, 69(2):2195–2203, Feb. 2020.

[57] X. Tan, S. Su, X. Guo, and X. Sun. Application of MIMO-OFDM technology in UAV communication network. In *World Symposium on Artificial Intelligence (WSAI)*, pages 1–4, Guangzhou, 2020.

[58] D. Wu and N. Ansari. High capacity spectrum allocation for multiple D2D users reusing downlink spectrum in LTE. In *IEEE International Conference on Communications (ICC)*, pages 1–6, May. Kansas City, MO, 2018.

[59] D. Wu, X. Sun, and N. Ansari. A cooperative drone assisted mobile access network for disaster emergency communications. In *IEEE Global Communications Conference (GLOBECOM)*, pages 1–6, Dec. Waikoloa, HI, 2019.

[60] S. Yamaguchi, H. Watanabe, H. Yoshioka, Y. Morimoto, H. Nakamizo, K. Tsutsumi, S. Shinjo, S. Uchida, A. Okazaki, T. Fukasawa, and N. Yoneda. Development of 28GHz band massive MIMO antenna RF frontend module for 5G. In *IEEE International Symposium on Antennas and Propagation USNC/URSI National Radio Science Meeting*, pages 629–630, Boston, MA, 2018.

[61] K. Yang, T. Jiang, Y. Shi, and Z. Ding. Federated learning via over-the-air computation. *IEEE Transactions on Wireless Communications*, 19(3):2022–2035, 2020.

[62] J. S. Yeom, Y. Kim, and B. C. Jung. UAV-assisted cooperative downlink NOMA with virtual full-duplex operation. In *Eleventh International Conference on Ubiquitous and Future Networks (ICUFN)*, pages 4–6, Agreb, 2019.

[63] C. Zah, H. Zhang, Y. Jia, L. Cai, H. Zhang, V. Wirth, K. Luan, W. Gu, W. Wang, and X. Liu. Low smile vertically stacked laser bars enable kw modular line lasers. In *IEEE High Power Diode Lasers and Systems Conference (HPD)*, pages 9–10, Oct. Coventry, 2017.

[64] S. Zhang and N. Ansari. 3D drone base station placement and resource allocation with FSO-based backhaul in hotspots. *IEEE Transactions on Vehicular Technology*, 69(3):3322–3329, Mar. 2020.

[65] Z. Zhao, Z. Zhang, J. Tan, Y. Liu, and J. Liu. 200 Gb/s FSO WDM communication system empowered by multiwavelength directly modulated TOSA for 5G wireless networks. *IEEE Photonics Journal*, 10(4):1–8, Aug. 2018.